Article

SOURCE DATA | TRANSPARENT PROCESS

EMBO reports

Inositol-requiring enzyme-1 regulates phosphoinositide signaling lipids and macrophage growth

Syed Muhammad Hamid[1], Mevlut Citir[2], Erdem Murat Terzi[3], Ismail Cimen[4,5], Zehra Yildirim[1,6,7], Asli Ekin Dogan[1,6,7], Begum Kocaturk[8], Umut Inci Onat[6,7], Moshe Arditi[1,8], Christian Weber[4,5,9,10], Alexis Traynor-Kaplan[11,12], Carsten Schultz[2,13] & Ebru Erbay[1,14,*]

Abstract

The ER-bound kinase/endoribonuclease (RNase), inositol-requiring enzyme-1 (IRE1), regulates the phylogenetically most conserved arm of the unfolded protein response (UPR). However, the complex biology and pathology regulated by mammalian IRE1 cannot be fully explained by IRE1's one known, specific RNA target, X box-binding protein-1 (XBP1) or the RNA substrates of IRE1-dependent RNA degradation (RIDD) activity. Investigating other specific substrates of IRE1 kinase and RNase activities may illuminate how it performs these diverse functions in mammalian cells. We report that macrophage IRE1 plays an unprecedented role in regulating phosphatidylinositide-derived signaling lipid metabolites and has profound impact on the downstream signaling mediated by the mammalian target of rapamycin (mTOR). This cross-talk between UPR and mTOR pathways occurs through the unconventional maturation of microRNA (miR) 2137 by IRE1's RNase activity. Furthermore, phosphatidylinositol (3,4,5) phosphate ($PI(3,4,5)P_3$) 5-phosphatase-2 (INPPL1) is a direct target of miR-2137, which controls $PI(3,4,5)P_3$ levels in macrophages. The modulation of cellular $PI(3,4,5)P_3/PIP_2$ ratio and anabolic mTOR signaling by the IRE1-induced miR-2137 demonstrates how the ER can provide a critical input into cell growth decisions.

Keywords ER stress; microRNA; mTOR signaling; hyperlipidemia; macrophage
Subject Categories Signal Transduction; RNA; Molecular Biology of Disease
DOI 10.15252/embr.202051462 | Received 4 August 2020 | Revised 19 September 2020 | Accepted 22 September 2020 | Published online 2 November 2020
EMBO Reports (2020) 21: e51462

See also: **T Avril & E Chevet** (December 2020)

Introduction

Endoplasmic reticulum (ER) plays an essential role in protein folding, lipid synthesis, and cellular calcium homeostasis. The disruption of ER's functions can induce an adaptive stress response, known as the unfolded protein response (UPR). The mammalian UPR is an elaborate cellular signaling initiated at the ER membranes that involves transcriptional and translational layers geared to reinstate cellular homeostasis (Ron & Walter, 2007; Schuck *et al*, 2009; Tabas & Ron, 2011; Walter & Ron, 2011). Inositol-requiring enzyme-1 (IRE1), one of the three proximal ER stress sensors sitting on the ER membranes, senses misfolded proteins through its ER luminal domain, leading to IRE1 oligomerization and activation of its kinase and endoribonuclease (RNase) activities that reside in its cytoplasmic domain. On the other hand, the incorporation of saturated fatty acids (SFA) or free cholesterol leads to another type of ER stress known as the lipid bilayer stress and sensed by IRE1 transmembrane domain, leading to IRE1 oligomerization and activation (Volmer *et al*, 2013; Volmer & Ron, 2015). Although ER plays a central role in lipid metabolism (cholesterol and phospholipid synthesis, fatty acid desaturation), ER membranes are poor in cholesterol and SFA content (Hotamisligil & Erbay, 2008; Walter & Ron, 2011). As such, the ER membrane is not only uniquely poised to sense the changes in cellular cholesterol and SFA levels, but also sufficiently equipped with lipid-sensing transcription factors and key lipid metabolism enzymes to maintain membrane lipid

1 Smidt Heart Institute, Cedars-Sinai Medical Center, Los Angeles, CA, USA
2 The Cell Biology and Biophysics Unit, European Molecular Biology Laboratory, Heidelberg, Germany
3 Department of Pathology, Laura and Isaac Perlmutter Cancer Center, New York University School of Medicine, New York, NY, USA
4 Institute for Cardiovascular Prevention (IPEK), Ludwig-Maximilians-University, Munich, Germany
5 German Center for Cardiovascular Research (DZHK), Partner Site Munich Heart Alliance, Munich, Germany
6 Department of Molecular Biology and Genetics, Bilkent University, Ankara, Turkey
7 National Nanotechnology Center, Bilkent University, Ankara, Turkey
8 Departments of Pediatrics and Medicine, Division of Infectious Diseases and Immunology, and Infectious and Immunologic Diseases Research Center, Department of Biomedical Sciences, Cedars-Sinai Medical Center, Los Angeles, CA, USA
9 Department of Biochemistry, Cardiovascular Research Institute Maastricht (CARIM), Maastricht University, Maastricht, The Netherlands
10 Munich Cluster for Systems Neurology (SyNergy), Munich, Germany
11 Department of Medicine, University of Washington School of Medicine, Seattle, WA, USA
12 ATK Innovation, Analytics and Discovery, North Bend, WA, USA
13 Department of Chemical Physiology and Biochemistry, Oregon Health and Science University, Portland, OR, USA
14 Departments of Cardiology, Department of Biomedical Sciences, Cedars-Sinai Medical Center, Los Angeles, CA, USA
*Corresponding author. Tel: +1 310 4237483; E-mail: ebru.erbay@cshs.org

equilibrium (Lee *et al*, 2003). As we have previously shown, ER membrane fatty acid saturation index provides a critical input for IRE1 oligomerization on the ER membranes and IRE1 activation state *in vivo* (Cimen *et al*, 2016). Moreover, IRE1, through its RNase activity's target, the X box-binding protein-1 (XBP1), regulates the expression of key phospholipid metabolism enzymes. A well-known role of yeast Ire1 involves monitoring and promoting phosphatidylinositol (PI) levels, but no such regulation has been reported in mammalian cells (Chang *et al*, 2002). A zebrafish mutant that is defective in *de novo* PI synthesis exhibits overt ER stress and develops hepatosteatosis, but how UPR is connected to PI metabolism has not been investigated beyond yeast (Thakur *et al*, 2011).

De novo PI synthesis is known to be crucial for intracellular availability of phosphatidylinositol 4,5-biphosphate ($PI(4,5)P_2$) and phosphatidylinositol 3,4,5-trisphosphate ($PI(3,4,5)P_3$) and proper functioning of downstream growth-promoting signaling pathways regulated by these lipids (Rameh & Mackey, 2016; Fruman *et al*, 2017). PI is synthesized in the ER and transported to other cellular membranes and phosphorylated and dephosphorylated by kinases and phosphatases to yield phosphatidylinositol phosphates (PIP_n). Depending on the phosphorylation state, different protein effectors are recruited to regulate the signaling events. For example, $PI(3,4,5)P_3$ recruits AKT serine/threonine kinase-1 (AKT) to the plasma membrane, where AKT is phosphorylated (on Serine 473) by the mammalian target of rapamycin complex-2 (mTORC2; Shimobayashi & Hall, 2014; Manning & Toker, 2017). Upon activation, AKT induces mTORC1-regulated anabolic signaling through 70-kDa ribosomal S6 protein kinase-1 (p70S6K) and eukaryotic translation initiation factor 4E-binding protein (4E-BP1), leading to increased protein synthesis and growth (Mehrpour *et al*, 2010; Zoncu *et al*, 2011; Knaevelsrud & Simonsen, 2012).

Numerous studies have shown mTOR signaling shares extensive cross-talk with the UPR, but how this contributes to mammalian cell growth is not clear (Wullschleger *et al*, 2006; Rutkowski & Hegde, 2010; Zoncu *et al*, 2011; Tabas & Ron, 2011; Appenzeller-Herzog & Hall, 2012). A common stimulus that controls both mTOR and UPR is the availability of nutrients and growth signals (Hotamisligil, 2010). For example, SFA that are prevalent in obese persons activate both UPR and mTOR (Pineau & Ferreira, 2010). Also, UPR-mediated lipogenesis has been reported to be mTORC1-dependent in the obese mouse liver (Pfaffenbach *et al*, 2010). The collective evidence indicates that the UPR and mTOR can act synergistically to regulate cell growth, but no such direct link has been reported yet.

A tight control of PIP_n signaling lipid levels is critical for a spatiotemporally regulated signaling mechanism (Balla *et al*, 2009; Kim *et al*, 2011). In this study, we analyzed the impact of IRE1 on the production of PIP_n signaling lipids from the ER-synthesized PI in macrophages. The results of our lipidomic analysis did not support a role for the mammalian IRE1 in the regulation of cellular PI production, however, we made the striking observation that IRE1's RNase activity significantly impacts cellular $PI(3,4,5)P_3$ levels. Our data further show that IRE1 RNase activity generates microRNA miR-2137, that leads to post-transcriptional inhibition of a lipid phosphatase INPPL1 ($PI(3,4,5)P_3$ 5-phosphatase-2 (INPPL1) and accumulation of $PI(3,4,5)P_3$ in bone marrow-derived macrophages (BMDM). The inhibition of IRE1 RNase activity or miR-2137 reduces macrophage cell size and proliferation in accord with the suppression of AKT-mTOR signaling. These results demonstrate IRE1-generated miR-2137 modulates an ER to plasma membrane, $PI(3,4,5)P_3$-dependent, anabolic signaling that contributes to mammalian cell growth decision.

Results

Ablating macrophage IRE1 RNase activity can significantly reduce $PI(3,4,5)P_3$ and downstream growth signaling

We previously demonstrated that targeting IRE1's RNase activity with a highly specific, small molecule inhibitor, 4μ8c, inhibits only its RNase activity and effectively prevents macrophage inflammation and atherosclerosis progression in mice (Tufanli *et al*, 2017). Similar to other cells, in macrophages, UPR arms display basal signaling activity (assessed by sXBP1—a read out for IRE1 activity and glucose regulated protein-78 (GRP78)—a read out for activating transcription factor-6 (ATF6)-regulated UPR arm) without stress induction, and this basal IRE1 RNase signaling can be inhibited by 4μ8c (Fig EV1A and B). Traditionally, UPR has been studied under acute ER stress conditions induced by chemical ER toxins (such as thapsigargin and tunicamycin), but very little is known about the basal IRE1 signaling in cells and tissues and its consequences (Iwawaki *et al*, 2004; Hayashi *et al*, 2007; Brunsing *et al*, 2008; Iwawaki *et al*, 2009; Cretenet *et al*, 2010; Onat *et al*, 2019). Due to its atherosclerosis promoting functions, there is a great interest in understanding IRE1 signaling in macrophages and as it relates to macrophage biology. In this study, we set out to investigate the role of basal IRE1 RNase activity in the metabolism of PI and PI-derived signaling lipids by using a quantitative lipidomics approach in non-stressed BMDMs (Traynor-Kaplan *et al*, 2017). We observed that the inhibition of IRE1 RNase activity with a specific inhibitor, 4μ8c, did not alter cellular PI levels, however, we noted a striking reduction in the cellular $PI(3,4,5)P_3$ to PIP_2 ratio (Figs 1A, and EV1C and D). The decrease in $PI(3,4,5)P_3$ to $PI(3,4)P_2$ was also confirmed by ELISA (Fig EV1E). Moreover, the ratio of cellular $PI(3,4,5)P_3$ to PI and to PIP (Figs 1B and C, and EV1F and G) was also decreased upon IRE1 RNase inhibition. As expected, the spliced form of XBP1 (sXBP1) mRNA expression, a direct RNA substrate and a measure of IRE1 RNase activity, was also significantly reduced by 4μ8c treatment in the analyzed cells (Fig EV1H). This finding reveals an unprecedented role for IRE1 in the regulation of PI-derived signaling lipids in macrophages.

We next tried to gain insight into the biological consequences of reduced $PI(3,4,5)P_3/PIP_2$ ratio in IRE1-inhibited cells. Decreased level of $PI(3,4,5)P_3$ can inhibit the phosphorylation of AKT and its downstream target mTORC1, which further phosphorylates p70S6K and 4E-BP1 (Ben-Sahra & Manning, 2017). The phosphorylation of AKT, p70S6K, S6 and 4E-BP1 were all inhibited in the IRE1 RNase inhibitor-treated BMDMs (Fig 1D).

We further assessed this cross-talk *in vivo* using peritoneal macrophages isolated from mice that were injected with an ER toxin (tunicamycin—an inhibitor of protein N-linked glycosylation),and treated with or without 4μ8c (Gomez & Rutkowski, 2016; Harnoss *et al*, 2019). This acute ER stress resulted in IRE1 activation (evident

by an increase in IRE1 phosphorylation and sXBP1 mRNA levels) and increased phosphorylation of p70S6K, S6 and 4E-BP1, which was significantly blocked by 4μ8c (Fig 1E). sXBP1 was also partially reduced by 4μ8c (Fig EV1I). This result shows IRE1-dependent regulation of the mTOR signaling pathway by ER stress also occurs *in vivo*.

To confirm IRE1-dependent regulation of mTOR signaling, we next analyzed this pathway in BMDMs that were obtained from mice with myeloid-specific IRE1 gene deletion (IRE1$^{-/-}$; *IRE1*$^{flox/flox}$, LysM cre$^{+/+}$) and compared with BMDMs obtained from age-matched, control littermates (IRE$^{+/+}$; *IRE1*$^{flox/flox}$) (Iwawaki *et al*, 2009). In these cells, ER bilayer membrane stress and IRE1 activity was induced by treating with a SFA, palmitate (PA) (Wei *et al*, 2006; Diakogiannaki *et al*, 2008; Ishiyama *et al*, 2011; Tufanli *et al*, 2017). We observed that non-stressed BMDMs from IRE1$^{-/-}$ mice displayed significantly lower p70S6K phosphorylation, in

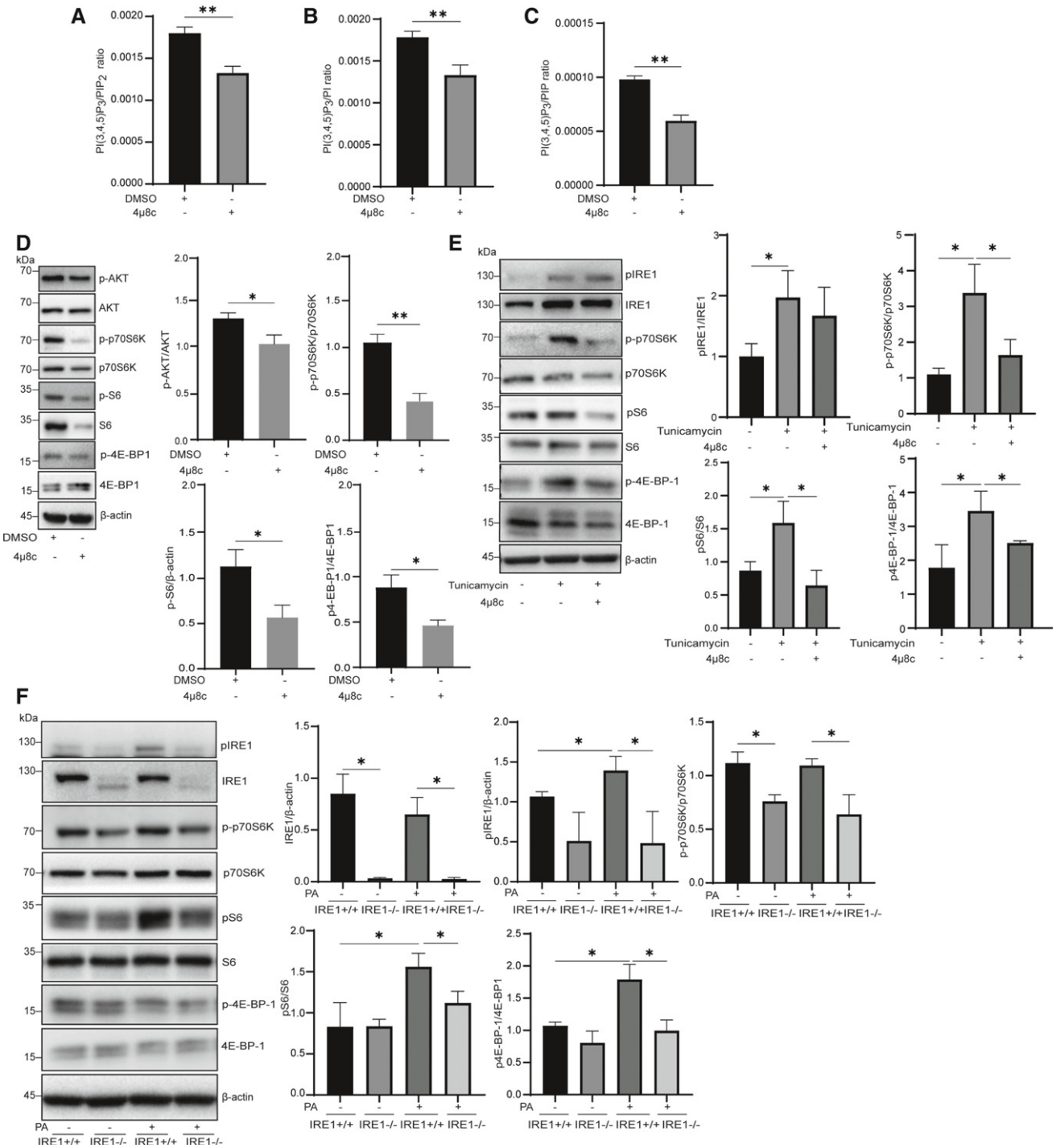

Figure 1.

Figure 1. Inhibition of IRE1 RNase activity leads to significant reduction in PI(3,4,5)P_3 and downstream growth signaling.

A–C Bone marrow-derived mouse macrophages (BMDMs) from wild type C57BL/6 mice were treated with 4μ8c (100 μM) or vehicle (dimethyl sulfoxide; DMSO) for 24 h prior to sample processing for lipidomics analysis: (A) PI(3,4,5)P_3 to PIP_2; (B) PI(3,4,5)P_3 to PI; (C) PI(3,4,5)P_3 to PIP ratio are shown. Data represent mean values ± standard error of mean (SEM) of peak areas normalized to internal standards ($n = 3$ biological replicates).

D BMDMs were treated with 4μ8c (100 μM) or DMSO for 24 h and protein lysates were analyzed by Western blotting using specific antibodies against, pAKT^{S473}, AKT, p70S6K^{T389}, p70S6K, pS6$^{S235/236}$, S6, p4E-BP1^{S65}, 4E-BP1, and β-actin. Western blot quantifications are shown next to the figure ($n = 3$ biological replicates; a representative blot is shown).

E Wild type C57BL/6 mice were injected with tunicamycin (1 mg/kg) and 4μ8c (10 μg/kg) for 8 h prior to sacrifice and collection of thiogylcolate-elicited peritoneal macrophages. Protein lysates were analyzed by Western blotting using specific antibodies against, pIRE1^{S742}, IRE1, pAKT^{S473}, AKT, p70S6K^{T389}, p70S6K, pS6$^{S235/236}$, S6, p4E-BP1^{S65}, 4E-BP1, and β-actin ($n = 3$ biological replicates; a representative blot is shown). Western blot quantifications are shown next to the figure.

F IRE1$^{+/+}$ and IRE1$^{-/-}$ BMDMs were treated with PA (500 μM) for 6 h, and protein lysates were analyzed by Western blotting using specific antibodies against pIRE1^{S742}, IRE1, p70S6K^{T389}, p70S6K, pS6$^{S235/236}$, S6, p4E-BP1^{S65}, 4E-BP1 and β-actin. Western blot quantifications are shown next to the figure ($n = 3$ biological replicates, a representative blot is shown).

Data information: All data are mean ± SEM; ($n = 3$). Unpaired *t*-test with Welch's correction. *$P \leq 0.05$, **$P \leq 0.01$.

comparison to BMDMs from IRE1$^{+/+}$ mice (Fig 1F). PA activated IRE1 (as evident by IRE1 autophosphorylation) and AKT-mTOR signaling, but this was significantly reduced in the IRE1$^{-/-}$ BMDMs when compared to IRE1$^{+/+}$ BMDMs, confirming our findings obtained with the IRE1 RNase inhibitor (Fig 1F). In alignment with the important function of p70S6K and S6 in cell growth and protein synthesis, inhibition of IRE1 RNase domain by 4μ8c resulted in a significant decrease in protein synthesis and cell size (in BMDMs) (Fig EV1J and K). Collectively, these findings reveal a novel role for IRE1's RNase activity in regulating PI-derived signaling lipids in macrophages.

IRE1-dependent miRNA expression changes in palmitate-stressed macrophages

The role of *IRE1-XBP1* in regulating phospholipid synthesis is conserved from yeast to mammals, but this is not the case in regulating PI production (Walter & Ron, 2011), Another striking difference between yeast Ire1 and mammalian IRE1 is that the latter was shown to alter the expression of a select group of ER stress-induced microRNA (miRNAs) (Upton *et al*, 2012). Many other studies have shown ER stress can either induce or reduce the expression of miRNAs, but a direct contribution of IRE1 to miRNA generation has not been illuminated (Behrman *et al*, 2011; Maurel & Chevet, 2013; Acosta-Alvear *et al*, 2018). We hypothesized that IRE1-regulated miRNAs may play a role in mediating IRE1's novel regulatory function in PI-derived signaling lipid metabolism. For this, we utilized primary BMDMs from IRE$^{-/-}$ and IRE1$^{+/+}$ mice that were either stressed with PA (to induce IRE1 activity) or not stressed (to assess basal IRE1 activity) and their respective impact on miRNA expression. RNA isolated from these BMDMs was analyzed for changes in miRNA differential expression using a microarray platform and the PA upregulated miRNAs in IRE1$^{+/+}$ are shown along with their corresponding levels in IRE$^{-/-}$ cells (Fig 2A). The PA downregulated miRNAs in IRE1$^{+/+}$ and their corresponding expression in IRE$^{-/-}$ cells are also shown (Appendix Fig S1). Based on this analysis, miR-2137 was the highest, induced miRNA by PA in IRE1$^{+/+}$ BMDMs. A smaller, but not significant, induction of miR-2137 was observed in the IRE1$^{-/-}$ BMDMs. We further confirmed IRE1-dependent upregulation of miR-2137 by PA in these cells by quantitative reverse transcriptase polymerase chain reaction (qRT–PCR) method (Fig 2B). In conjunction with findings from a previously published study that showed two different chemical ER toxins induce miR-2137, our results demonstrate miR-2137 is responsive to multiple modes of ER stress activation and is regulated by IRE1 (Behrman *et al*, 2011). In our experiment, PA induced IRE1 kinase activity (as assessed by IRE1 phosphorylation) and only one of the IRE1 RNase outputs, XBP1 mRNA splicing, but not the other, RIDD activity (as evident from the unchanged mRNA levels of the Biogenesis of Lysosome-Related Organelles Complex-1 Subunit-1 (BLOC1S1) and Scavenger Receptor Class-A Receptor-3 (SCARA3)) (Fig 2C–F). Collectively, these results show that IRE1 RNase activation leads to a significant increase in miR-2137 expression in BMDMs.

miR-2137 is also regulated by hyperlipidemia-induced IRE1 *in vivo*

Saturated and monounsaturated fatty acids (MUFA) reprogram gene expression in different ways to alter macrophage functions (Duplus *et al*, 2000). Whereas SFA can induce ER stress response, MUFA do not (Wei *et al*, 2006; Diakogiannaki *et al*, 2008; Ben-Dror & Birk, 2019). While miR-2137 is induced by SFA like PA and stearic acid (SA) in BMDMs, it cannot be induced with MUFA such as palmitoleic acid (PAO) and oleic acid (OA) (Fig 3A). sXBP1 mRNA, a measure of IRE1 RNase activity, paralleled the changes in miR-2137 levels in these treatments (Fig 3B). These results suggest that miR-2137 expression (similar to IRE1 oligomerization and RNase activity) is responsive to the degree of fatty acid saturation in BMDMs (Volmer *et al*, 2013; Volmer & Ron, 2015; Cimen *et al*, 2016).

Obesity and high-fat diets also lead to persistent ER stress (and IRE1 activation) in many organs and in lipid-laden, foamy macrophages (Kawasaki *et al*, 2012; Pagliassotti *et al*, 2016). A high-SFA- and cholesterol-containing diet is a major risk factor for the development of cardiovascular disease (Wang & Hu, 2017). To confirm miR-2137 regulation by lipids also occurs *in vivo*, we isolated peritoneal macrophages from chow diet or high-fat/high-cholesterol diet (Western diet; WD)-fed mice (for 16 weeks). While WD can induce mild hypercholesterolemia in wild type (WT) mice, WD feeding in mice lacking the apolipoprotein E gene (Apoe$^{-/-}$) can result in marked increases in plasma lipid levels (> 1,000 mg/dl; Getz & Reardon, 2012). Moreover, peritoneal macrophages isolated from hypercholesterolemic mice are loaded with lipids, display UPR activation and secrete inflammatory cytokines, highly similar to the lipid-laden, foamy macrophages found in atherosclerotic plaques (Li *et al*, 2004; Oh *et al*, 2012; Moore *et al*, 2013; Fig EV2A and B). In comparison to peritoneal macrophages obtained from chow diet-fed

WT mice, peritoneal macrophages obtained from WD-fed mice showed a significant induction of IRE1 and miR-2137 (Figs 3C and EV2A). Consistently, peritoneal macrophages obtained from WD-fed Apoe$^{-/-}$ mice also displayed significantly higher IRE1 activity and miR-2137 levels when compared to macrophages isolated from chow diet-fed Apoe$^{-/-}$ mice (Figs 3D and EV2B). These findings demonstrate miR-2137 expression and IRE1 activation are co-regulated by hyperlipidemia in peritoneal macrophages *in vivo*. Next, we sought evidence for IRE1's role in regulating miR-2137 *in vivo* and analyzed miR-2137 levels in peritoneal macrophages from Apoe$^{-/-}$ mice that were fed with WD (to induce IRE1 activation) and treated with the IRE1 RNase inhibitor, 4μ8c (Tufanli *et al*, 2017). Inhibition

A

Micro RNA up-regulated by palmitate treatment		
	IRE1$^{+/+}$	IRE1$^{-/-}$
miRNA	Fold Change (Log2)	Fold Change (Log2)
mmu-miR-2137	2.08	NS
mmu-miR-12197-3p	1.3	1.5
mmu-miR-6937-5p	1.16	NS
mmu-miR-762	1.15	NS
mmu-miR-5126	0.86	NS
mmu-miR-3963	0.55	NS
mmu-miR-7a-5p	0.51	NS
mmu-miR-7b-5p	0.44	NS
mmu-miR-23-3p	0.12	NS

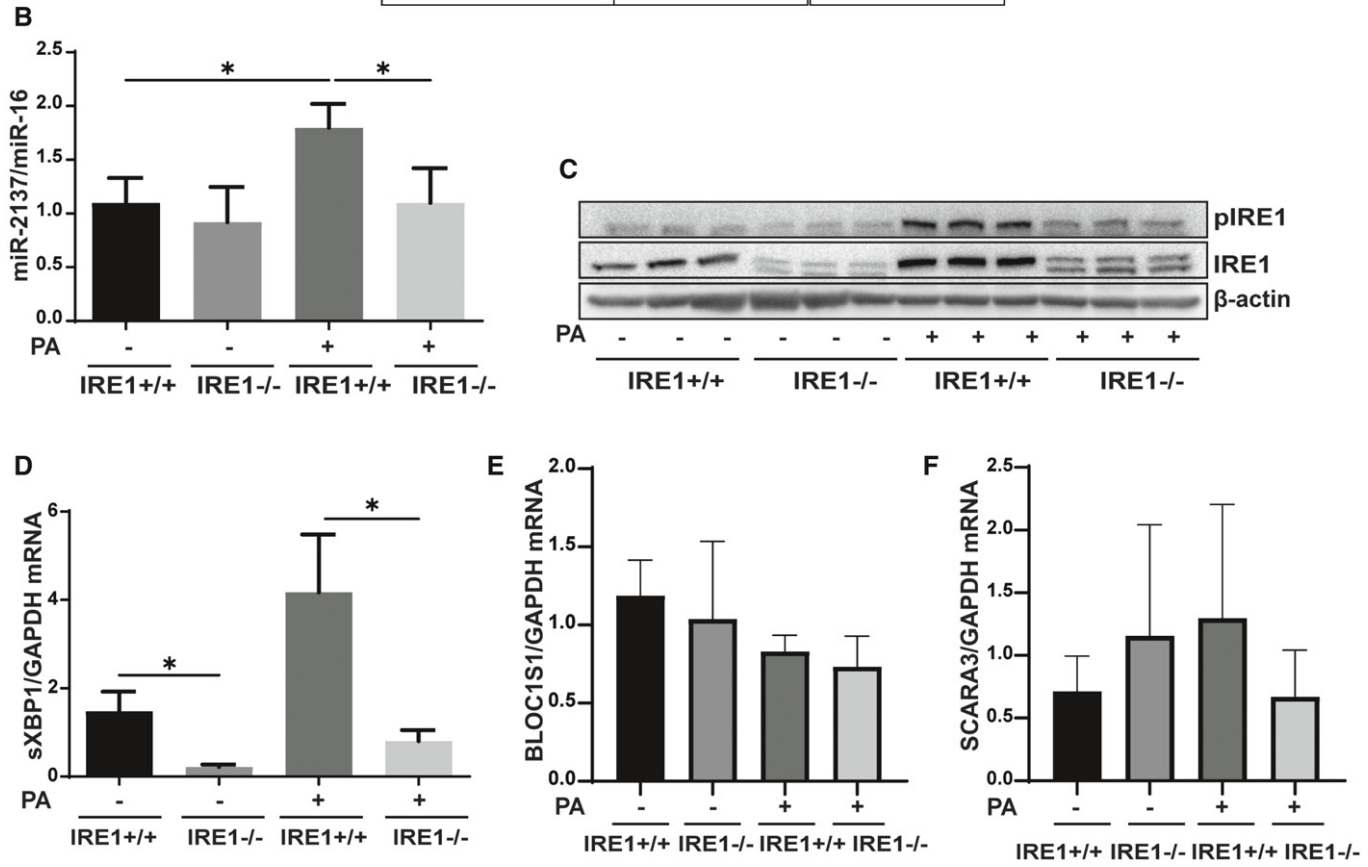

Figure 2.

Figure 2. IRE1-dependent changes in miRNA expression in ER-stressed macrophages.

A IRE1$^{-/-}$ and IRE1$^{+/+}$ BMDMs were treated with PA (500 μM) or vehicle for 6 h prior to RNA isolation for miRNA analysis using a microarray platform. Table showing fold change (log_2) of statistically significant (P-value < 0.050) top PA-upregulated miRNAs in IRE1$^{+/+}$ and IRE1$^{-/-}$ cells. NS indicates microRNAs that did not show statistically significant difference. Fold change was calculated by comparing mean intensity values of microarray signal for vehicle treatment with PA treatment (n = 3 biological replicates).

B RNA lysates from the same experiment were analyzed by qRT–PCR for miR-2137 expression.

C Protein lysates were analyzed by Western blotting using specific antibodies for pIRE1^{S742}, IRE1, and β-actin (n = 3 biological replicates).

D RNA lysates were analyzed by qRT–PCR for sXBP1 expression (n = 3 biological replicates).

E, F RNA lysates from the same experiment were analyzed by qRT–PCR for (E) BLOC1S1 and (F) SCARA3 expression (n = 3 biological replicates).

Data information: All data are mean ± SEM (n = 3); unpaired t-test with Welch's correction; *$P \leq 0.05$).
Source data are available online for this figure.

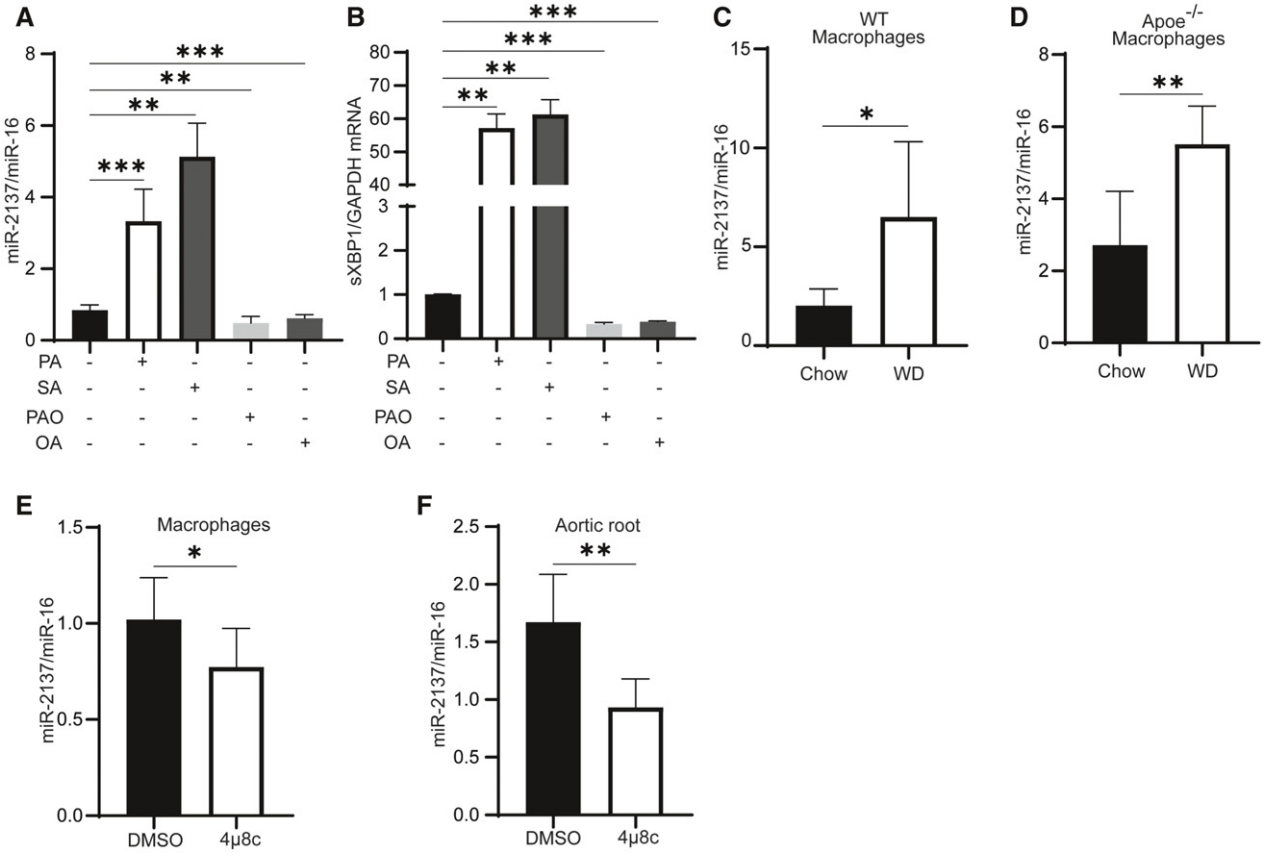

Figure 3. miR-2137 is regulated by IRE1 RNase activity *in vivo*.

A, B BMDMs were treated with PA, stearic acid (SA), palmitoleic acid (PAO), or oleic acid (OA) (500 μM) for 16 h. RNA lysates were analyzed by qRT–PCR for the expression of (A) miR-2137 and (B) sXBP1 (n = 3 biological replicates).

C, D (C) C57BL/6 (WT) and (D) Apoe$^{-/-}$ mice were fed with chow or WD for 16 weeks followed by peritoneal macrophage isolation. RNA lysates were analyzed by qRT–PCR for miR-2137 expression (WT; n = 4-4 mice per group, Apoe$^{-/-}$; n = 5-5 mice per group).

E, F Apoe$^{-/-}$ mice were fed with chow or WD for 16 weeks and injected with 4μ8c (10 mg/kg/day) or vehicle (DMSO) in the final 4 weeks of the diet (n = 5–7 mice per group): (E) RNA lysates from bone marrow were analyzed by qRT–PCR for miR-2137 expression (n = 5–7 mice per group). (F) Total RNA isolated from the aortic root plaques was analyzed by qRT–PCR for miR-2137 expression (n = 5–7 mice per group).

Data information: Data are mean ± SEM; unpaired t-test with Welch's correction. *$P \leq 0.05$, **$P \leq 0.01$, ***$P \leq 0.001$.

of IRE1's RNase activity by 4μ8c treatment *in vivo* significantly reduced miR-2137 expression in the peritoneal mouse macrophages (Fig 3E) as well as in the aortic root plaque area, enriched with lipid-laden, foamy macrophages (Fig 3F). The corresponding vascular lesions to these 4μ8c-treated aortic plaque samples were characterized in detail in our previously published study, which demonstrated 4μ8c treatment leads to a significant reduction in atherosclerosis progression (Tufanli *et al*, 2017). These findings

provide strong *in vitro* and *in vivo* support for IRE1's role in miR-2137 induction by ER stress.

miR-2137 maturation by IRE1's RNase activity

Upon observing co-regulation of miR-2137 and IRE1 RNase activity by lipids, we next investigated whether IRE1 is directly involved in the regulation of miR-2137 expression. For this, BMDMs were transfected with a silencer RNA (siRNA) specific for IRE1 and treated with PA (6 or 9 h). Both IRE1 protein and sXBP1 mRNA were significantly reduced by IRE1 siRNA treatment (Fig EV3A and B). Suppression of IRE1 expression significantly reduced PA-induced miR-2137 expression (Fig 4A). Additionally, the IRE1 RNase inhibitor, 4μ8c, significantly reduced both PA-induced and tunicamycin-induced sXBP1 mRNA and miR-2137 expression in BMDMs (Figs 4B and C, EV3C and D). These results show IRE1's RNase function is critical for robust miR-2137 induction during ER stress, yet they do not rule out the possibility that other UPR arms (which would not be inhibited by 4μ8c or IRE1 siRNA treatment) also contribute.

We further confirmed our observation that IRE1 RNase activity is involved in miR-2137 regulation by using IRE1-deficient ($IRE1^{-/-}$) mouse embryonic fibroblasts (MEF). PA treatment led to a smaller

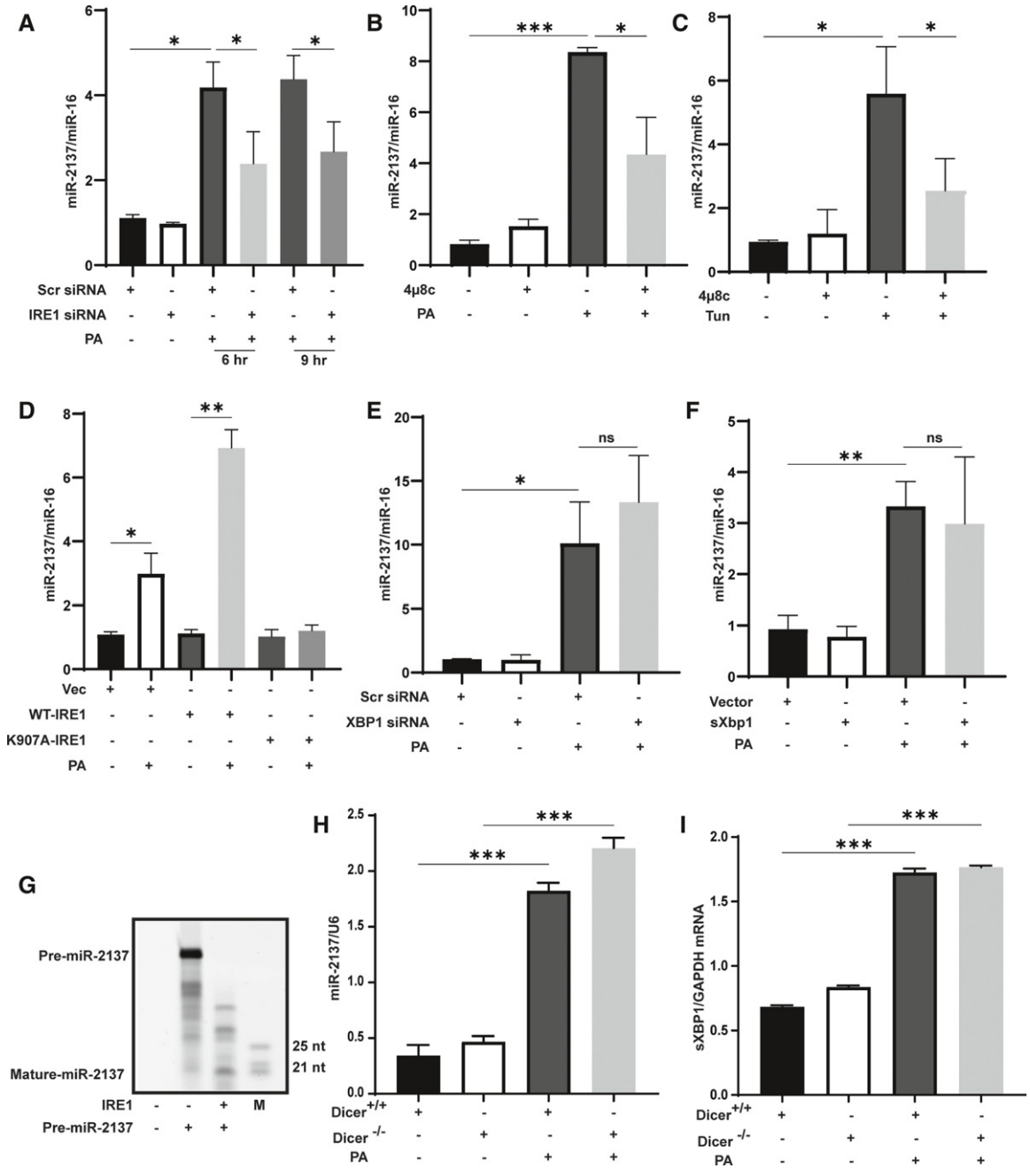

Figure 4.

Figure 4. miR-2137 is regulated by IRE1 RNase activity.

A BMDMs were transfected with scrambled (Scr) or IRE1-specific siRNA (40 nM) and treated with palmitate (PA, 500 μM) or vehicle for 6 and 9 h. RNA lysates were analyzed by qRT–PCR for miR-2137 expression (n = 3 biological replicates).

B BMDMs were treated with PA (500 μM) and 4μ8c (100 μM) or vehicle for 9 h. RNA lysates were analyzed by qRT–PCR for miR-2137 expression (n = 3 biological replicates).

C BMDM cells were treated with tunicamycin (Tun; 5 μg/ml) and 4μ8c (100 μM) or vehicle (DMSO) for 9 h. RNA lysates were analyzed by qRT–PCR for miR-2137 expression (n = 3 biological replicates).

D IRE1$^{-/-}$ MEFs were transfected with vector (control), WT-IRE1 or K907A-IRE1 (RNase-dead mutant) plasmids for 24 h, followed by PA (500 μM) treatment for 9 h. RNA lysates were analyzed by qRT–PCR for miR-2137 expression (n = 3 biological replicates).

E BMDMs were transfected with scrambled or XBP-1-specific siRNA (70 nM) for 24 h, followed by treatment with PA (500 μM) for 16 h. RNA lysates were analyzed by qRT–PCR for miR-2137 expression (n = 3 biological replicates).

F XBP1$^{-/-}$ MEFs were transfected with empty vector or sXBP1 plasmid for 24 h, followed by PA (500 μM) treatment for 9 h. RNA lysates were analyzed for miR-2137 expression by qRT–PCR (n = 3 biological replicates).

G IRE1 cleavage assay performed using synthetic pre-miR-2137 (50 nM) as substrate with active, recombinant IRE1 (100 ng) at 37°C for 2 h, followed by sample separation in Urea-PAGE and detection with SYBR gold staining. M indicates microRNA marker.

H, I BMDMs isolated from Dicer$^{+/+}$and Dicer$^{-/-}$ mice were treated with PA (500 μM) for 12 h. RNA lysates were analyzed by qRT–PCR for (H) miR-2137 and (I) sXBP1 expression (n = 3 biological replicates).

Data information: All data are mean ± SEM (n = 3); unpaired t-test with Welch's correction. *$P \leq 0.05$, **$P \leq 0.01$, ***$P \leq 0.001$.
Source data are available online for this figure.

increase in miR-2137 levels in the IRE$^{-/-}$ MEFs, suggesting other factors also contribute to miR-2137 expression in fibroblasts. However, reconstitution with wild type (WT) IRE1, but not with an RNase-dead IRE1 (K907A) mutant, drove miR-2137 expression to a significantly higher level (Figs 4D, and EV3E and F). These results show that IRE1 amplifies ER-stress-induced miR-2137 expression in both BMDMs and MEFs. Furthermore, these data demonstrate that a functional IRE1 RNase domain is critical for miR-2137 induction by ER stress.

Next, we investigated how IRE1 induces miR-2137 levels in cells. IRE1 RNase has two well-defined functions—splicing of XBP1 mRNA and RIDD activity (Walter & Ron, 2011; Moore & Hollien, 2015). PA induced miR-2137 levels in parallel to sXBP1 mRNA induction in BMDMs (Fig 2B and D). However, PA did not induce IRE1 RIDD activity in the same cells (Fig 2E and F). IRE1 RIDD activity is associated with degradation of its RNA substrates such as pre-miR-17 and reduction in miR-17 levels (Upton *et al*, 2012). Therefore, IRE1 RIDD activity is predicted to lead to the opposite outcome (a reduction in miR-2137) than the one we observe (induction of miR-2137) in ER-stressed cells. We therefore, focused on dissecting sXBP1's role in the observed increase of miR-2137 levels upon IRE1 activation. siRNA-mediating silencing of sXBP1 expression in BMDMs significantly reduced sXBP1 mRNA and its transcriptional target Endoplasmic Reticulum DNA J Domain-Containing Protein 4 (Erdj4) but did not prevent PA-induced miR-2137 production (Figs 4E, and EV3G and H). We further investigated whether sXBP1 overexpression could drive miR-2137 production. Reconstitution of sXBP1 in XBP1$^{-/-}$ MEFs induced Erdj4 mRNA but did not drive basal or PA-induced miR-2137 expression further (Figs 4F, and EV3I and J). These results demonstrate that miR-2137 induction by PA occurs independent of sXBP1.

Our findings led us to the intriguing possibility that IRE1's RNase activity may be directly involved in the cleavage of pre-miR-2137 and promote its maturation to miR-2137. We approached this question by designing an *in vitro* cleavage experiment using recombinant IRE1 and synthetic pre-miR-2137 in RNase cleavage buffer. In this assay we used XBP1 mRNA mini-stem loop as a positive control for specific IRE1 RNase activity. In our *in vitro* assay conditions, the recombinant IRE1 cleaved XBP1 mRNA mini-stem loop, demonstrating that IRE1 RNase activity is intact (Fig EV3K). We used additional controls to validate our experimental results such as excluding pre-miR-2137 from the reaction mix as well as doing the reaction in the presence of a heat-inactivated recombinant IRE1 protein. In both of these control conditions, there was no pre-miR-2137 cleavage that produced the mature form of miR-2137. In this reaction, only the active form of recombinant IRE1 cleaved pre-miR-2137, resulting in an RNA fragment that corresponds to the mature-sized miR-2137 (Figs 4G and EV3L). These findings show IRE1 can directly cleave pre-miR-2137 and produce a mature-sized miR-2137 product.

Since Dicer is a critical endoribonuclease involved in the processing of pre-miRNAs into mature miRNAs (Bartel, 2004), we next investigated whether PA-induced miR-2137 expression is dependent on Dicer. For this purpose, we used BMDMs obtained from either wild type for Dicer but lacking Apoe gene (*Dicer*$^{+/+}$; *Dicer*$^{flox/flox}$; *Apoe*$^{-/-}$ and *Apoe*$^{-/-}$ mice) or myeloid-specific Dicer-deficient (*Dicer*$^{-/-}$; *Dicer*$^{flox/flox}$, *LysM*$^{cre+}$, *Apoe*$^{-/-}$) mice (Wei *et al*, 2018). We confirmed Dicer mRNA expression was significantly suppressed in these BMDMs (Fig EV3M). miR-2137 levels were equally upregulated in both Dicer$^{+/+}$ and Dicer$^{-/-}$ BMDMs after PA treatment (Fig 4H), whereas let-7c-5p, a Dicer-dependent miRNA, was significantly reduced in the Dicer$^{-/-}$ BMDMs (Fig EV3N). In the same experiment, PA efficiently induced sXBP1 mRNA levels in both Dicer$^{+/+}$ and Dicer$^{-/-}$ BMDMs, demonstrating there is no apparent differences in IRE1 RNase activation by PA in these cells (Fig 4I). Collectively, our findings show that ER stress leads to IRE1-dependent yet Dicer-independent upregulation of miR-2137 expression in BMDMs.

INPPL1 is a target of miR-2137 in macrophages

We next sought to determine the biological target(s) of miR-2137 using microRNA target prediction programs such as miRanda and Diana Tools (Betel *et al*, 2008; Betel *et al*, 2010; Reczko *et al*, 2012; Paraskevopoulou *et al*, 2013). The three top targets identified for miR-2137 were Fas-activated serine/threonine kinase (FastK), Inositol Polyphosphate Phosphatase Like-1 (Inppl1) and latent transforming growth factor beta binding protein 3 (Ltbp3) (Fig

EV4A). We next studied INPPL1 as a putative target of miR-2137 in macrophages. INPPL1 is also known as the src homology 2 (SH2)-domain containing PtdIns(3,4,5)P_3 5-phosphatase-2 (SHIP2), and specifically hydrolyzes the phosphate on the 5′ position of the inositol ring, producing PtdIns(3,4)P_2 from PtdIns(3,4,5)P_3 (Elong Edimo *et al*, 2016). The analysis of 3′ untranslated region (UTR) of Inppl1 and miR-2137 seed sequence shows that they align with only one mismatch on the conserved seed sequence (Fig 5A). To confirm that miR-2137 regulates 3′ UTR of INPPL1, a luciferase reporter vector expressing 3′ UTR of INPPL1 was co-transfected with a miRNA mimic for miR-2137 or miR-205 (positive control: a previously published miRNA regulator of Inppl1 3′ UTR in mammalian cells) (Yu *et al*, 2008). Overexpression of either miR-2137 or miR-205 resulted in a significant decrease in Inppl1's 3′ UTR-controlled translation of the luciferase protein (Figs 5B, and EV4B and C). Moreover, overexpression of either miRNA in BMDMs led to a robust decrease in the protein levels of INPPL1 (Figs 5C, and EV4D and E). To further confirm miR-2137-dependent regulation of INPPL1, we next utilized an antagomir that is specific for miR-2137. Consistent with our earlier observations, treatment of BMDMs with PA induced endogenous miR-2137 expression and simultaneously led to a significant reduction in INPPL1 protein expression. Furthermore, inhibition of miR-2137 with its specific antagomir prevented PA-induced reduction in INPPL1 protein expression (Figs 5D and EV4F). These results demonstrate PA-induced miR-2137 can suppress INPPL1 expression in BMDMs.

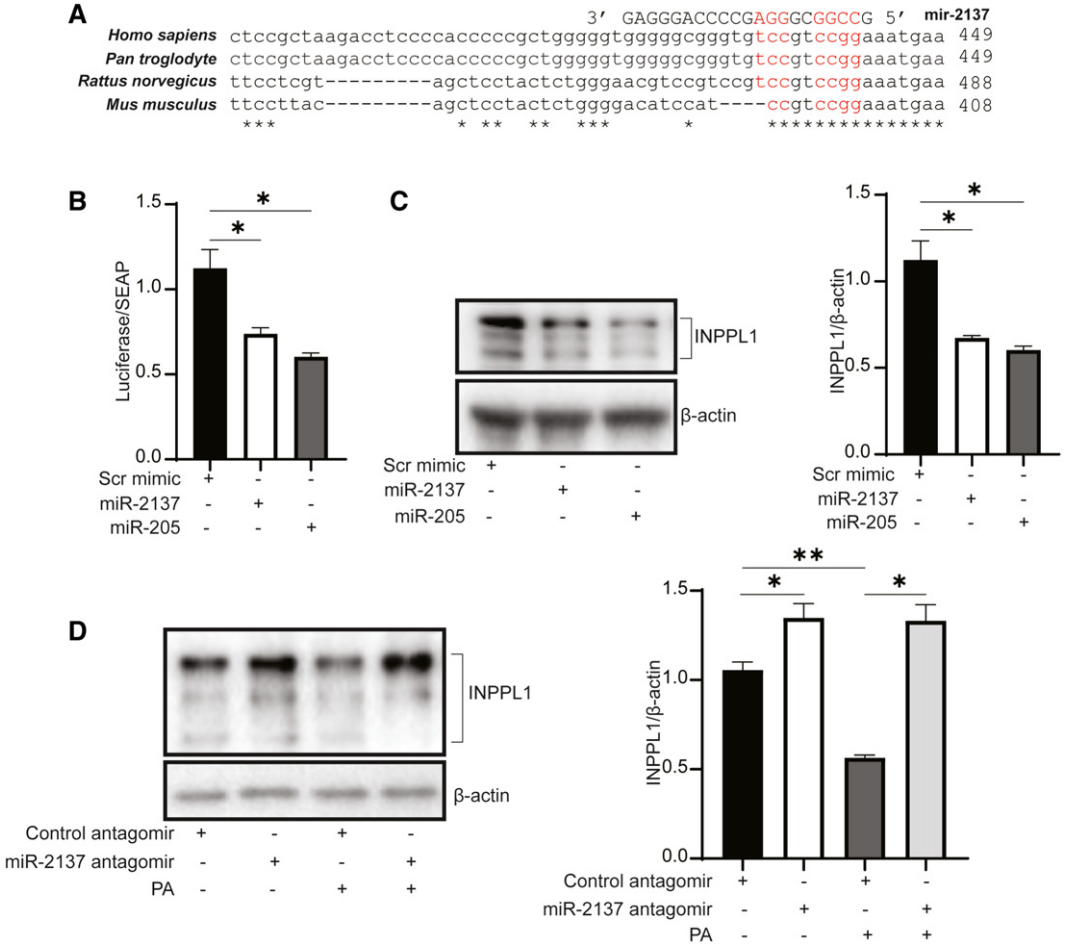

Figure 5. INPPL1 is a target for miR-2137.

A Putative miR-2137 binding site on 3′ UTR of human (Gene ID 3636), chimpanzee (Gene ID 451403), rat (Gene ID 65038), and mouse (Gene ID 16332) INPPL1 mRNA.

B HEK293 cells were co-transfected with an INPPL1 3′ UTR-luciferase plasmid and scrambled miRNA mimic (40 nM), miR-2137 mimic (40 nM), or miR-205 mimic (40 nM) for 24 h. Protein lysates were analyzed for luciferase activity and normalized to secreted embryonic alkaline phosphatase (SEAP) reporter activity (n = 3 biological replicates).

C BMDMs were transfected with scrambled miRNA mimic (40 nM), miR-2137 mimic (40 nM), and miR-205 mimic (40 nM) for 48 h, and protein lysates were analyzed by Western blotting using specific antibodies for INPPL1 and β-actin. Protein quantifications are displayed in graph next to the blots (n = 3 biological replicates).

D BMDMs were transfected with negative control antagomir (200 nM) or miR-2137 antagomir (200 nM) for 24 h, followed by PA (500 μM) treatment for 9 h. Protein lysates were analyzed by Western blotting using specific antibodies for INPPL1 and β-actin. Protein quantifications shown in the graph next to blots (n = 3 biological replicates).

Data information: All data are mean ± SEM (n = 3); unpaired t-test with Welch's correction. *$P \leq 0.05$, **$P \leq 0.01$.

miR-2137 regulates PI(3,4,5)P_3 levels and growth signaling in macrophages

Our findings show that IRE1 through miR-2137 signaling leads to suppression of INPPL1 protein expression, unraveling a novel link between IRE1 and phosphatidylinositol lipids metabolism. To confirm that the observed effect of miR-2137 on INPPL1 protein reflects actual changes in PtdIns levels, we performed a lipidomics analysis in BMDMs, in which we attempted to suppress INPPL1's lipid phosphatase activity by overexpressing miR-2137 or miR-205 (positive control). Indeed, overexpression of mimics for either miR-2137 or miR-205 led to a profound increase in PI(3,4,5)P_3 to PIP_2 ratio in BMDMs (Figs 6A and EV5A–D). The ratio of PI(3,4,5)P_3 to PI or PIP were also increased upon overexpression of both miR-2137 and miR-205 (positive control; known to suppress INPPL1 and thereby induce PI(3,4,5)P_3 levels) (Figs 6B and C, and EV5E and F) (Yu *et al*, 2008). These findings, in conjunction with INPPL1 protein reduction by miR-2137, clearly show miR-2137 regulates phosphatidylinositol phosphate signaling lipid metabolism in macrophages.

We next tried to gain insight into the biological consequences of altered miR-2137 levels in cells. INPPL1 hydrolyzes PI(3,4,5)P_3 to PI(3,4)P_2 at the plasma membrane and can inhibit the recruitment of AKT and its activation by phosphorylation (on Serine 473) by mTORC2, one of the two distinct protein complexes formed by mTOR (Backers *et al*, 2003; Huang & Manning, 2009). Phosphorylation and activation of AKT leads to activation of the mTORC1 complex that is further downstream. mTORC1 is well known for its regulatory function in cellular anabolism and protein synthesis, which is mediated by its direct substrates, 70-kDa ribosomal protein S6 kinase(p70S6K) and eukaryotic initiation factor 4E-binding protein (4E-BP1) (Kunz *et al*, 1993; Hara *et al*, 1998; Huang & Manning, 2009). It was also confirmed that INPPL1 overexpression in mice results in decreased AKT phosphorylation and downstream signaling *in vivo* (Kagawa *et al*, 2008). Here, we explored the possibility that miR-2137-dependent regulation of INPPL1 could modulate AKT signaling in BMDMs. We observed overexpression of miR-2137 mimic in BMDMs led to a decrease in INPPL1 protein levels with a corresponding increase in AKT phosphorylation as well as p70S6K, S6 and 4E-BP1 phosphorylation, downstream of AKT-mTORC1 (Figs 6D and EV5G). The addition of wortmannin, an inhibitor of PI3K/AKT pathway to the miR-2137 mimic overexpressing cells prevented this miR-2137 driven downstream mTORC1-dependent signaling (Fig EV5H; Manning & Cantley, 2007). Conversely, the inhibition of miR-2137 with a specific antagomir upregulated INPPL1 protein levels while decreasing the phosphorylation of AKT, p70S6K, S6, and 4E-BP1 (Figs 6E and EV5I). As our data show AKT-mTOR signaling is regulated by IRE1 (Fig 1) and this signaling promotes cell proliferation and growth, we next sought to determine the impact of the IRE1-induced miR-2137 on proliferation and growth of macrophages (Wullschleger *et al*, 2006; Ben-Sahra & Manning, 2017). Our analysis showed miR-2137 overexpression led to increased proliferation (of RAW264.7 macrophages) and protein synthesis rate and cell growth (in BMDMs) (Fig EV5J–M), whereas miR-2137-specific antagomir led to significantly reduced proliferation (of RAW264.7 macrophages) and protein synthesis rates (in BMDMs) (Fig EV5O and P). These findings collectively confirm the impact of miR-2137 signaling on macrophage proliferation and growth.

Discussion

Our knowledge of mammalian IRE1 signaling and its consequences is largely based on its RNase activity and its specific substrate, XBP1 mRNA, or its RIDD substrates in ER-stressed cells (Walter & Ron, 2011). However, there are significant differences in the biology controlled by the yeast and mammalian IRE1 proteins including mammalian IRE1's role in promoting inflammation and control over lipid metabolism. Moreover, circadian regulation of basal IRE1 activity has been observed in liver cells, where it appears to be synced to cellular metabolism (Cretenet *et al*, 2010; Chaix *et al*, 2016; Carreras-Sureda *et al*, 2019). IRE1's function in a non-stress situation is not well understood, nor can be explained by its one known substrate in mammalian cells. These observations suggest a thorough exploration of its RNase and kinase substrates is necessary to obtain a comprehensive understanding of this master regulator in mammalian cells during stress and also in normal conditions.

Our findings show that macrophage IRE1 RNase activity and its direct cleavage product, miR-2137, modulates PI-derived signaling lipid levels and impacts cell proliferation, protein synthesis, and growth (Fig 7). This finding was unexpected. First, yeast Ire1 regulates PI production but has not been associated with further metabolism of the signaling lipids derived from PI (Henry *et al*, 2014). Second, yeast Ire1 is not known to have an impact on cell size (Henry *et al*, 2010). Yet, our findings are consistent with mammalian studies that showed UPR and growth signaling pathways converge in many ways. Based on these earlier studies, UPR and the AKT-mTOR growth signaling pathways can be viewed as synergistic (such as in lipid synthesis) or antagonistic (such as in ribosome biogenesis, translation and autophagy). These previous studies have positioned UPR both upstream and downstream of mTORC1. Not much is known about UPR's impact on mTORC2 other than mTORC2 is inhibited by chronic ER stress (Appenzeller-Herzog & Hall, 2012). While mammalian IRE1 is not traditionally considered among the key players in growth processes, our findings clearly demonstrate basal IRE1 activity modulates cellular PIP_3 levels and AKT activation through mTORC2-mediated Serine 473 phosphorylation. These findings in non-stressed cells demonstrate that IRE1 and AKT-mTOR signaling interact in cellular homeostasis. A physiological example that supports this notion is the post-prandial upregulation of IRE1 signaling by mTORC1 in liver (Pfaffenbach *et al*, 2010). Furthermore, IRE1's non-canonical role in promoting cell growth and proliferation (via miR-2137 induction and INPPL1 inhibition) and its canonical role in sensing misfolded proteins could work synergistically in immune cells and help mount a proper immune response. But it is also possible that these two IRE1 functions can unintentionally propagate chronic inflammation in pathological states such as obesity and hyperlipidemia, where IRE1 and miR-2137 are both induced (Hotamisligil, 2010 and our current study). Furthermore, IRE1's non-canonical function appears to be reminiscent of how ATF6 arm of the UPR promotes compensatory cardiac growth and proliferation in cancer (Schewe & Aguirre-Ghiso, 2008; Blackwood *et al*, 2019). It was shown that muscle growth, which entails increased protein synthesis and protein folding, is

accompanied with ATF6 activation and the induction of its target, Ras homologue enriched in brain (RHEB), a small GTPase that activates mTORC1 (Blackwood *et al*, 2019). Additionally, AKT-mTOR can also feedback inhibit IRE1 RNase activity. For example, AKT/mTOR signaling promotes ER-mitochondria contacts and the stabilization of the inter-organelle contacts suppresses IRE1's RNase

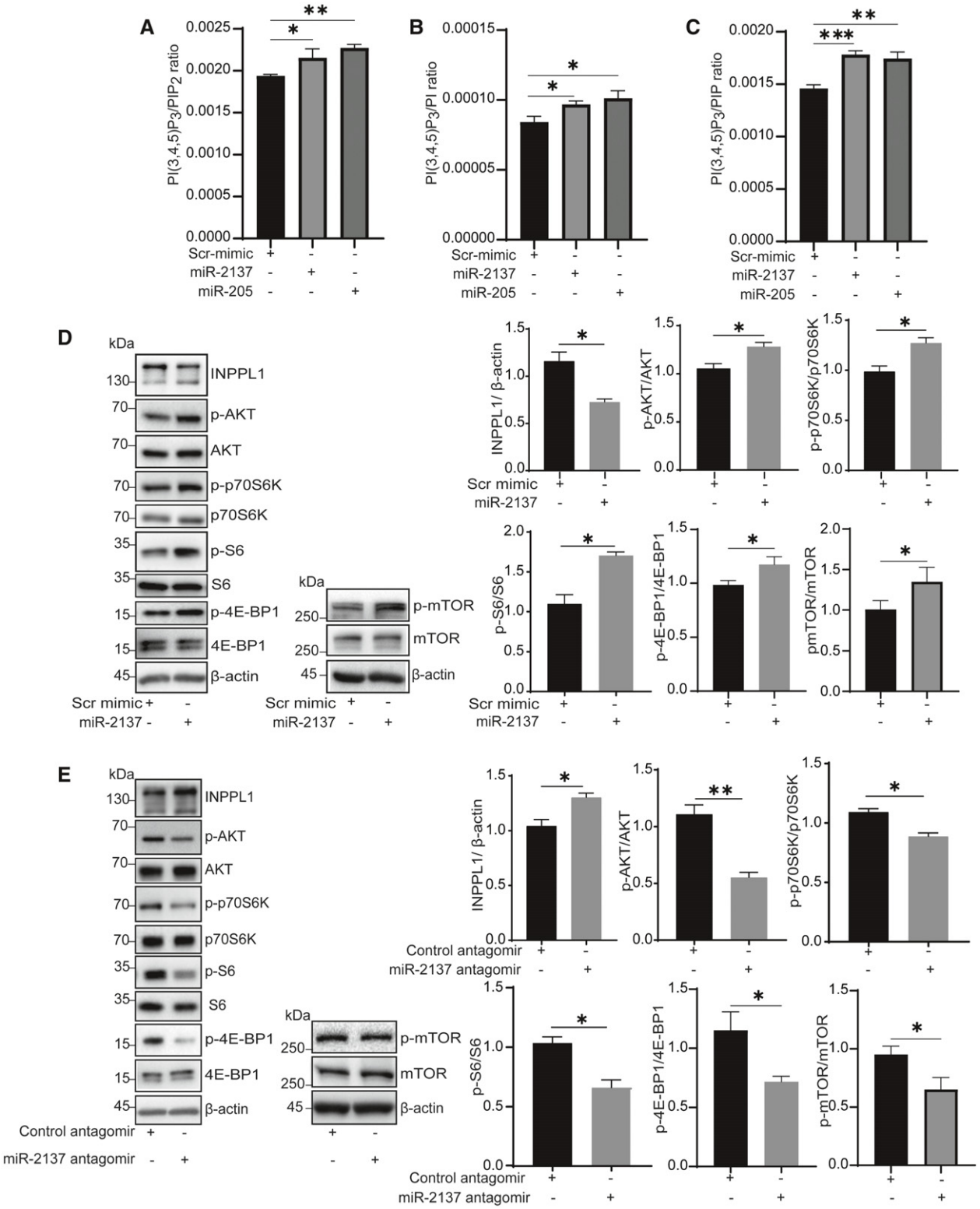

Figure 6.

Figure 6. miR-2137 regulates PI(3,4,5)P3/PIP2 ratio and growth signaling in macrophages.

A–C BMDMs were transfected with scrambled miRNA mimic (40 nM), miR-2137 mimic (40 nM) or miR-205 mimic (40 nM) for 24 h, and cells were processed for lipidomics analysis as described in Materials and Methods section. The ratio of lipids from this analysis is shown for (A) $PI(3,4,5)P_3$ to PIP_2; (B) $PI(3,4,5)P_3$ to PI; (C) $PI(3,4,5)P_3$ to PIP. Data from LC/MS/MS using a Waters Xevo TQ-S MS/MS in MRM mode represent mean values ± SEM of peak areas normalized to internal standards as described in Materials and Methods ($n = 3$ biological replicates).

D, E BMDMs were transfected with (D) scrambled miRNA mimic (40 nM) or miR-2137 mimic (40 nM) for 48 h and (E) with control antagomir (200 nM) or miR-2137 antagomir for 24 h, and protein lysates were analyzed by Western blotting using specific antibodies against INPPL1, $pAKT^{S473}$, AKT, $p70S6K^{T389}$, p70S6K, $pS6^{S235/236}$, S6, $p4E\text{-}BP1^{S65}$, 4E-BP1, $pmTOR^{S2448}$, mTOR, and β-actin. Protein quantifications are shown next to the Western blots ($n = 3$ biological replicates).

Data information: All data are mean ± SEM ($n = 3$); unpaired *t*-test with Welch's correction. $^*P \leq 0.05$, $^{**}P \leq 0.01$, $^{***}P \leq 0.001$.

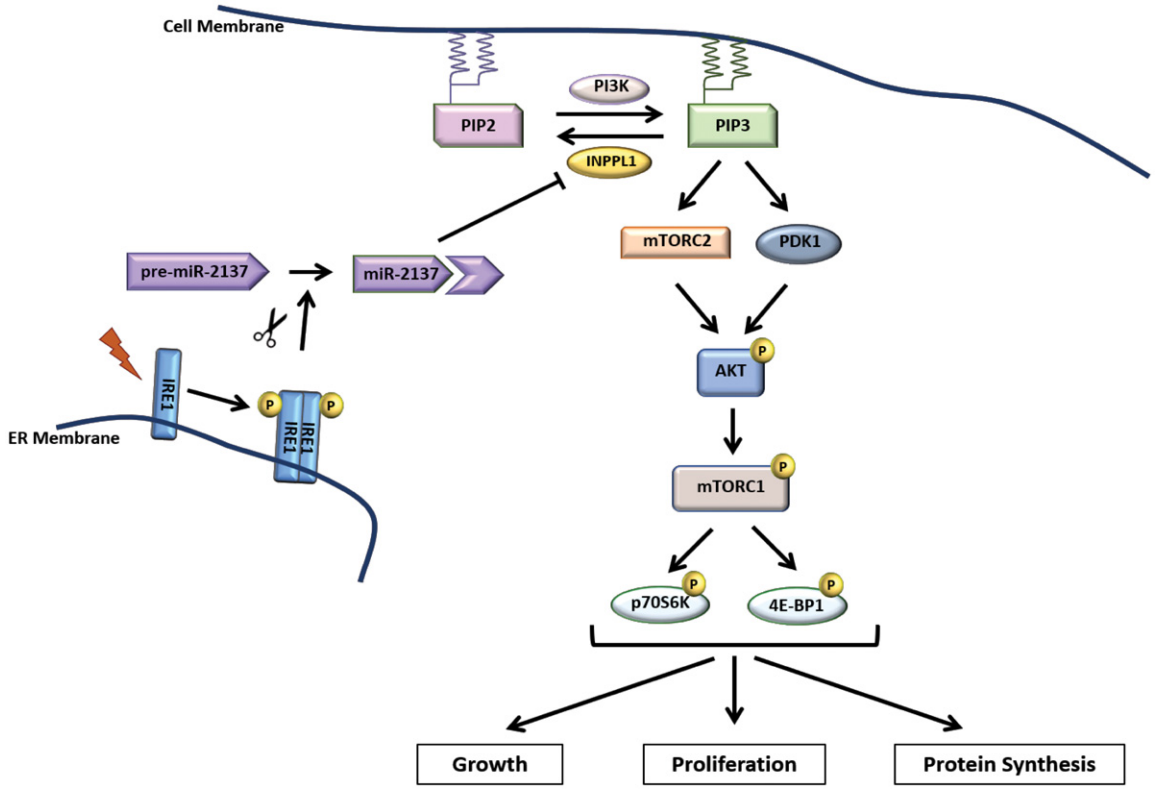

Figure 7. IRE1-miR-2137-INPPL1 axis in cell growth and proliferation.

The ER-anchored IRE1 RNase is directly involved in the maturation of miR-2137, which targets and downregulates INPPL1. The reduction in INPPL1 protein results in the accumulation of PIP3, recruiting AKT to the plasma membrane where it can be phosphorylated by mTORC2 complex. Activated AKT signals to mTORC1 complex, leading to phosphorylation of p70S6K and 4E-BP1 and induction of anabolic pathways that promote cell growth and proliferation.

activity (Sanchez-Alvarez *et al*, 2017). In summary, these earlier findings in conjunction with our current data that detail the intricate links between UPR and mTOR signaling in mammalian cells underscore ER's role in anabolic and growth decisions.

While the only known, specific RNA target for IRE1's RNase activity is XBP1 mRNA, it was also shown that IRE1 RNase activity degrades some ER-localized mRNAs (to reduce ER protein load) and specific pre-miRNAs through a process known as RIDD activity (Upton *et al*, 2012; Wang *et al*, 2018). All of these IRE1 RNase outputs are considered pro-survival mechanisms by way of mitigating ER stress. However, our data do not support a role for XBP1 or RIDD in IRE1-mediated miR-2137 maturation. Our findings show a third, unprecedented, direct role for IRE1 RNase activity in the generation of miR-2137. In the canonical miRNA biogenesis pathway, pre-miRNA is cleaved in the cytoplasm by Dicer, which interacts with Ago2, TAR RNA binding protein (TRBP) and the Protein activator of the interferon-induced protein kinase (PRKRA) in the RNA-induced silencing complex (RISC) (Bernstein *et al*, 2001; Chendrimada *et al*, 2005). While IRE1 does not associate with Dicer or Ago2, several other RNA binding proteins (RNAbp) found in the RISC complex were shown to be in physical interaction with IRE1 in both non-stress and ER stress conditions (Acosta-Alvear *et al*, 2018). Future studies will be necessary to unearth the details of IRE1's complex interactions with these RNA binding proteins found in the miRNA biogenesis machinery and the consequences on miR biogenesis or miR-mediated expression changes in cells.

Studies have shown Dicer-independent miRNA biogenesis pathways exist and microRNAs are still produced in Dicer knock out cells, albeit at reduced expression levels (Yang & Lai, 2011; Kim *et al*, 2016). The mechanism for only one of the Dicer-independent miRNAs, miR-451, has been discovered and involves the processing of pre-miR451 by Ago2 (Cheloufi *et al*, 2010). Although miR-2137 is annotated as a miRNA in all major databases, there are some indications that this might not be a canonical miRNA. A recent report shows miR-2137 is an Ago-independent microRNA (Kelly *et al*, 2019). Our findings on miR-2137 reveal a novel role of IRE1 RNase in the generation of a mature miRNA. Importantly, IRE1's involvement in miRNA maturation appears to be highly specific to miR-2137 (analogous to its one specific mRNA target, XBP1), at least in macrophages that we studied. However, there are no conserved IRE1-specific cleavage sequences on pre-miR-2137. Future detailed studies will be needed to define the exact IRE1-specific cleavage site on pre-miR-2137.

There could be further implications of IRE1-regulated phosphatidylinositol phosphate metabolism that was not addressed in our current study. For example, it is known that IRE1 is important for NLRP3 inflammasome activation, but the mechanisms are not fully understood (Tufanli *et al*, 2017). The assembly and activation of the NLRP3 inflammasome on trans Golgi network is guided by PI(4)P enriched on this endomembrane compartment (Chen & Chen, 2018). Given that IRE1 can modulate INPPL1 expression and PI(4)P is one of the products of INPPL1 activity, a possibility that remains to be explored is whether IRE1-mediated NLRP3 activation involves PI(4)P-dependent localization of NLRP3 to the Golgi. It is also plausible that the cellular $PI(4,5)P_2$ levels that are altered by IRE1 RNase-INPPL1 activity could impact ER calcium uptake from the plasma membrane (PM) as it is known that $PI(4,5)P_2$ concentration is important for both the membrane localization and activity of the PM-ER calcium channels (Chung *et al*, 2017). A deeper understanding of the regulation of PI-derived signaling lipids by the mammalian IRE1 in future studies can potentially expand the IRE1 signaling beyond the traditional boundaries of UPR signaling in yeast.

Our findings also show that miR-2137 levels can be significantly induced by SFA and ER stress in macrophages *in vitro* and *in vivo*. SFA treatment of macrophages *in vitro* and high-fat diets in mice *in vivo* also induce IRE1 activity (Zhou *et al*, 2006; Volmer *et al*, 2013; Halbleib *et al*, 2017). High-fat diet-induced hyperlipidemia is linked to increased inflammation, hepatosteatosis, atherosclerosis and insulin resistance (Kanda *et al*, 2006; Riera-Borrull *et al*, 2017; Zhao *et al*, 2018). Previously, we showed that inhibiting IRE1 RNase activity reduces atherosclerosis progression in mice (Tufanli *et al*, 2017). Our current data confirm that hyperlipidemia-induced IRE1 RNase activity is also responsible for the induction of miR-2137 production in macrophages and in the atherosclerotic plaques *in vivo* (Cimen *et al*, 2016; Tufanli *et al*, 2017). Whether IRE1-induced miR-2137 production contributes to atherogenesis is an intriguing possibility that needs to be tested in future studies. Finally, significant induction of miR-2137 has been documented in ischemia in several tissues (such as heart and the nervous system) whereas IRE1 activation in ischemic conditions is regarded as having a protective outcome (Zhou *et al*, 2013; Ueno *et al*, 2016; Liu *et al*, 2016; Ni *et al*, 2018; Wu *et al*, 2019). Therefore, an alluring prospect for utilizing the growth-promoting effects of miR-2137 may involve promoting the survival of the affected tissue in ischemia.

In summary, we report an unprecedented regulatory role of IRE1 in PI-derived signaling lipids metabolism, which involves first-of-a-kind IRE1-generated mature miRNA, miR-2137. Our findings demonstrate IRE1-miR2137-INPPL1 signaling axis can relay an anabolic message originating from the ER to the signaling pathways that assemble on the plasma membrane to govern cell growth and proliferation.

Materials and Methods

Reagents and plasmids

$IRE1^{-/-}$, $XBP1^{-/-}$ and wild type (WT) mouse embryonic fibroblasts (MEF) were a kind gift from Dr. Gokhan Hotamisigil (Harvard University, T.H. Chan School of Public Health, Boston). pCMV-Xbp1, WT-Ire1-pcDNA3, and RNase-dead IRE1 mutant (K907A)-pcDNA3 plasmids were a kind gift from Dr. Peter Walter (University of California, San Francisco). For 3′ untranslated region (UTR) analysis; control vector (CmiT000001-MT05), Inppl1 3′UTR expression vector (MmiT093023-MT05, NM 010567.2) and Secrete-pair dual luminescence assay kit (LF031) were purchased from GeneCopoeia. Fatty acid-free bovine serum albumin (BSA) was purchased from Gold Biotechnology (A-421-250). Polyethylinimine (PEI; molecular weight 25,000) was purchased from Polysciences (23966) and used for transfection of plasmids to MEFs. Neon electroporation system was purchased from Thermo Scientific and used with Neon transfection system 100 μl kit (MPK10096) according the previously published electroporation protocols suitable for BMDM or RAW264.7 macrophages (Tufanli *et al*, 2017, Onat et al, 2019). L-Glutamine, Dulbecco's modified Eagle's Medium (DMEM), phosphate buffer saline (PBS), Hank's balanced salt solution (HBSS), penicillin/streptomycin (P/S), fetal bovine serum (FBS), Roswell Park Memorial Institute (RPMI)-1640 medium, Vybrant® MTT Cell Proliferation Assay Kit (3-(4,5-dimethylthiazol-2-yl)-2,5-diphenyltetrazolium bromide (MTT; M6494), mirVana miRNA negative control mimic (4464059), mirVana-miR-2137 (4464067, Assay ID MC15897) and mirVana-miR-205 (4464066, Assay ID MC11015) mimics were purchased from Thermo Scientific. Trypsin, ampicillin, palmitic acid (PA; P0500), protease inhibitor cocktail (P8340) and phosphatase inhibitor cocktail-3 (P0044), dimethyl sulfoxide (DMSO; D8418) were purchased from Sigma. The IRE1 RNase inhibitior, 4μ8c, was purchased from Calbiochem (412512). Palmitoleate (PAO, U-40-A), stearic acid (SA, N-18HY-A), and oleic acid (OA, U-46-A) were purchased from Nu-Chek. Primary antibodies used for immunoblotting were purchased from the following companies: Anti-phospho-S724 IRE1 (124945) and Inppl1 (70267) antibodies from Abcam; IRE1 antibody (3294), phospho-S473-AKT (9271), AKT (9272S), phospho-T389-p70S6K (9203), p70S6K (9202), phospho-S6-S235/236 (2211), S6 (2217), phospho-S65-4E-BP1 (9451), phospho T980-pPERK (3179), and PERK (3192) were from Cell-Signaling; β-Actin-horse radish peroxidase (47778) was from Santa Cruz Biotechnology. miScript inhibitor negative control (1027272), anti-mmu-miR-2137 miRNA inhibitor (MIN0011213, Product No. 219300), IRE1 siRNA (SI00995883), Xbp1 siRNA (SI01473227), and all-star negative control scrambled siRNA (1027281) were purchased from Qiagen.

Primary macrophage isolation and culture

Bone marrow-derived macrophages

Bone marrows were collected from mouse tibia and femur bones into RPMI containing %1 Penicillin/streptomycin (P/S) cocktail. Briefly, after filtering through a 70 μm pore sized cell strainer (BD Biosciences; 352350), cells were centrifuged at 500 *g* for 5 min and resuspended in RPMI enriched with %20 L929 cells' conditioned medium and %1 P/S, followed by growth on plastic petri dishes (not cell culture-grade) and differentiation to macrophages for 5 days, as previously described (Tufanli *et al*, 2017).

Peritoneal macrophages

Mice were injected (intraperitoneal) with 3% thioglycolate solution (Sigma; 70157) and peritoneal macrophages were collected 4 days after by washing the peritoneal cavity with 10 ml ice-cold PBS, as previously described (Zhang *et al*, 2008; Onat *et al*, 2019). The peritoneal macrophages were centrifuged at 500 *g* for 5 min at + 4°C and resuspended in RPMI medium prior to seeding on cell culture-grade plates. Macrophages were allowed to attach for 30 min and the other non-adherent cells (not macrophages) were washed away with media. Cells were rinsed several times with PBS and later used in experiments.

Immortalized cell line culture

RAW264.7 macrophages were maintained in RPMI supplemented with 10% FBS and 1% L-glutamine. MEFs and human embryonic kidney (HEK)-293T cells were maintained in DMEM supplemented with 10% FBS and 1% L-glutamine in a humidified, 5% carbon dioxide incubator at 37°C.

Palmitate/ bovine serum albumin complex preparation

PA was dissolved in absolute ethanol to yield a stock concentration of 500 mM and stored at −80°C. Stock PA was diluted to working concentration and suspended in serum free RPMI growth medium that contains 1% fatty acid-free BSA by mixing at 55°C for 15 min, as described earlier (Erbay *et al*, 2009).

Transfection and electroporation

60–80% confluent $Ire1^{-/-}$ and $Xbp1^{-/-}$ MEFs were transfected using polyethylenimine reagent by using 2 μg of plasmid DNA for 1×10^6 million cells as described previously (Tufanli *et al*, 2017).

RAW264.7 and BMDMs were electroporated using Neon electroporator (Thermo Scientific) as per specific conditions provided by the manufacturer for these cell types on its protocols' webpage and as described earlier (Tufanli *et al*, 2017). BMDMs were electroporated with IRE1 siRNA (50 nM), Xbp1 siRNA (70 nM), all-star negative control scrambled siRNA (at concentrations that match other siRNA treatments in the same experiment), mirVana-miR-2137 mimic (40 nM), mirVana-miR-205 mimics (40 nM) and scrambled miR miR (40 nM), miR-2137 antago-miR (200 nM) and scrambled antago-miR (200 nM) using the Neon electroporator (Thermo Scientific). Electroporation parameters for BMDMs were as following: voltage: 1,500, width: 20, pulse: 1. 24 h after transfection, cells were treated with 500 μM PA to induce ER stress RAW264.7 cells were transfected with microRNA mimic and antago-miR at same concentrations used for BMDMs by electroporation using the following parameters voltage: 1,680, width: 20, pulse: 1.

RNA isolation and quantitative reverse transcription polymerase chain reaction

Trizol reagent (Thermo Scientific) was used to isolate total RNA from all cell and tissue types. The RNA was reverse transcribed to cDNA using Revert-Aid First Strand complementary DNA (cDNA) synthesis kit (Thermo Scientific; K1691), according to manufacturer's protocol. Power-Up-SYBR green (Applied Biosystems; A25742) was used for the qRT–PCR reaction on Rotor Gene qRT-PCR machine (Qiagen). miScript II RT kit (Qiagen; 2128160) was used for miRNA expression analysis, according to manufacturer's instructions. miScript primer assay for miR-2137 (MS00021917), miR-16-2 (MS00024269), RNU6-2 (MS00033740), miR-let7c-5p (MS00005852) and for miR-205 (MS00001862) were purchased from Qiagen and miR expression analysis was performed using miScript Quantitec SYBR green PCR kit (Qiagen; 204143). The following PCR primers were used for mRNA expression analysis:

mmu-sXBP1-F 5′ TGAGAACCAGGAGTTAAGAACACGC 3′
mmu-sXBP1-R 5′ CCTGCACCTGCTGCGGAC 3′
mmu-GAPDH-F 5′ GTGAAGGTCGGTGTGAACG 3′
mmu-GAPDH-R 5′ GGTCGTTGATGGCAACAATCTC 3′
mmu-INPPL1-F 5′ ACTCTGCGTCCTGTATCAAAAG 3′
mmu-INPPL1-R 5′ CAGGGCACAAACAAGACCC 3′
mmu-DICER-F 5′-GAATAAGGCTTATCTTCTGCAGG-3′
mmu-DICER-R 5′-CATAAAGGTGCTTGGTTATGAGG-3′
mmu-ERDJ4-F 5′-CTCCACAGTCAGTTTTCGTCTT-3′
mmu-ERDJ4-R 5′-CGCCTTTTTGATTTGTCGCTC-3′
mmu-SCARA3-F 5′-TGACAGGGATGTACTGTGTGT-3′
mmu-SCARA3-R 5′-TGCAAAGATAGGTTCTTCTGGC-3′
mmu-BLOC1S1-F 5′-TCCCGCCTGCTCAAAGAAC-3′
mmu-BLOC1S1-R 5′-GAGGTGATCCACCAACGCTT-3′

miRNA profiling by microarray

BMDMs were treated with 500 μM PA or vehicle control for 6 h and total RNA was isolated using miRNeasy RNA isolation kit (Qiagen, 217004). RNA was quantified on Nanodrop 2000 (Invitrogen) and 2 μg used for the microarray analysis, which was carried out by LC Sciences (Texas, USA). Mouse miRbase 22 (March 2018) database was used in this analysis.

In vitro IRE1 RNA cleavage assay

Pre-miR-2137 (>mmu-mir-2137 MI0010750 GUAGUAUACCUCCUUCCUGCUGCCUUGUUGGCUUGCCGGCGGGAGCCCCAGGGAGUAGAGCAUUGC) and sXBP1 mini-stem loop (CUGAGUCCGCAGCACUCAG) were custom synthesized by IDT DNA technologies. Recombinant human IRE1 was purchased from SignalChem (E31-11G-05). The IRE1 cleavage reaction was carried out in cleavage assay buffer (containing 20 mM HEPES (pH 7.0), 50 mM NaCl and 1 mM DTT) with IRE1 (100 ng) and synthetic pre-miR-2137 (50 nM) or Xbp1 mini-stem loop at 37°C, according to previously

published protocols (Korennykh *et al*, 2011; Upton *et al*, 2012). The reaction was halted upon the addition of the RNA gel loading dye (Thermo) followed by heating at 95°C and immediate cooling on ice. The RNA cleavage products were then resolved on 12% urea-polyacrylamide gel (PAGE), stained with SYBR gold and imaged using ChemiDoc (Bio-Rad).

Flow cytometry

Cells were fixed using 4% paraformaldehyde for 10 min at room temperature, rinsed with PBS and collected in flow cytometry assay buffer (1% BSA in PBS). Cells were analyzed on BD LSR Fortessa flow cytometer (BD Biosciences). In order to eliminate debris, the acquired events were gated with forward scatter (FSC) and side scatter (SSC). Median FSC values were used to plot the graphs.

Proliferation assay

RAW 264.7 macrophages were electroporated with miRNA mimic or inhibitors and 24 h later, 1×10^4 cells were seeded on 96-well cell culture plates with phenol red-free DMEM that was supplemented with 10% FBS. After 24–48 h of growth, MTT assay was performed using Vybrant MTT Cell Proliferation Assay kit (M6494, Thermo Scientific). MTT (10 μl from 5 mg/ml working solution) was added to each well and incubated in 5% CO_2 and 37°C incubator for 4 h, according to the kit manual. DMSO was added to each well (150 μl) and the plate was gently shaken to dissolve the crystals. Optical density was measured at 540 nm using SpectraMax M2 microplate reader (Molecular Devices). Treatments were done in quadruplicates and repeated three times.

Mice studies and treatments

C57BL/6 (wild type) and Apolipoprotein E-deficient ($Apoe^{-/-}$) mice were purchased from Jackson laboratory. Starting at 8–10 weeks old, C57BL/6 and $Apoe^{-/-}$ mice were fed with normal chow or high-cholesterol/high-fat atherosclerotic mouse diet (0.21% cholesterol and 21% butter fat), obtained from Ssniff Spezialdiaten, Germany (corresponding to TD.88137 diet; catalog number: E15721) for 16 weeks. We re-examined atherosclerotic plaques from our previously published study: Briefly, we reported that these $Apoe^{-/-}$ mice received intraperitoneal injections of either 4μ8c (10 mg/kg/day) or vehicle, both delivered in 20% vol/vol cremophor-EL (Sigma) saline solution, for the duration of diet (Tufanli *et al*, 2017).

$Dicer^{flox/flox}$, $LysM^{cre}$ and $Apoe^{-/-}$ mice were purchased from Jackson Lab and inter-crossed. At 6–8 weeks of age these mice were utilized for BMDM isolation in the Institute for Cardiovascular Prevention, Ludwig Maximillians University in Munich, Germany (Wei *et al*, 2018).

IRE1 conditional knock out ($IRE1^{flox/flox}$) mice were a kind gift from Dr. Takao Iwawaki (Kanazawa Medical University, Japan) and characterized before (Iwawaki *et al*, 2009). $IRE1^{flox/flox}$ mice were inter-crossed from with $LysM^{cre}$ mice purchased from Jackson Lab (004781) to obtain $IRE1^{flox/flox}$; $LysM^{cre}$ mice, which had a myeloid-specific IRE1 gene deletion.

Study approval

All animal experiments were performed according to protocols approved by the Experimental Animal Ethical Care Committees at Bilkent University, Ankara, Turkey, Institute for Cardiovascular Prevention, LMU Munich, Germany or Cedars Sinai Medical Center, Los Angeles, USA.

In vitro protein synthesis assay

Cells were electroporated with miRNA mimic or inhibitor and 24 h later, they were seeded on 96-well, black, clear-bottom cell culture plates. Alternatively, the cells were first seeded on 96-well, black, clear-bottom, cell culture plates and 24 h later, treated with either dimethyl sulfoxide (DMSO) or 4μ8c (100 μM). Protein synthesis measurements were performed 24 h after electroporation or inhibitor treatment using a protein synthesis assay kit (Cayman; 601100) according to manufacturer's protocol.

Western blot analysis

Cells were lysed in a lysis buffer (50 mM HEPES (pH: 7.9), 100 mM NaCl, 10 mM EDTA, 10 mM sodium fluoride (NaF), 4 mM tetrasodium pyrophosphate ($Na_4P_2O_7$), 1% Triton, 2 mM Sodium orthovanadate (Na_3VO_4), 1 mM phenylmethanesulfonylfluoride (PMSF), 1× phosphatase inhibitor cocktail 3 and 1 × (10 μM/ml) protease inhibitor cocktail) as described in (Cimen *et al*, 2016). Lysates were cleared by brief centrifugation followed by the addition of sodium dodecyl sulfate (SDS)-loading dye and heated at 95°C for 5 min before loading on SDS-polyacrylamide gel (SDS–PAGE) gels. After separation according to protein molecular weights on these gels, samples were transferred to polyvinylidene difluoride (PVDF) membrane. Blocking and antibody incubation of the membranes were carried out in tris-buffered saline (TBS) buffer prepared with 0.1% Tween-20 (*v*/*v*) and 5% (*w*/*v*) dry milk or BSA. These membranes were developed in ECL prime reagent (Amersham) and images were captured with ChemiDoc (Bio-Rad).

Lipidomics analysis

Materials

Avanti Polar Lipids, PIP_3 37:4, PIP_2 37:4, PIP 37:4, PI 37:4, Eppendorf DNA LoBind 2 ml polypropylene microfuge tubes. Methanol, chloroform, dichloromethane, and acetonitrile (Fisher) were all of mass spectrometry grade. Sodium formate and HCl were from Sigma, and TMS-diazomethane (TMS-DM, 2.0 M in diethyl ether or hexanes) from Sigma-Aldrich and Acros. The lipid analytical internal standards were ammonium salts of 1-heptadecanoyl-2-(5Z,8Z,11Z,14Z-eicosatetraenoyl)-sn-glycero-3-phospho-(1′-myo-inositol-3′,4′,5′-trisphosphate) [17:0, 20:4 PI(3,4,5)P_2], 1-heptadecanoyl-2-(5Z,8Z,11Z,14Z-eicosatetraenoyl)-sn-glycero-3-phospho-(1′-myo-inositol-4′,5′-bisphosphate) [17:0, 20:4 PI(4,5)P_2]; 1-heptadecanoyl-2-(5Z,8Z,11Z,14Z-eicosatetraenoyl)-sn-glycero-3-phospho-(1′-myo-inositol-4′-phosphate) [17:0, 20:4 PI(4)P]; and 1-heptadecanoyl-2-(5Z,8Z,11Z,14Z-eicosatetraenoyl)-sn-glycero-3-phospho-(1′-myo-inositol) [17:0, 20:4 PI] from Avanti Polar Lipids (LIPID MAPS MS Standards).

Sample preparation and TCA precipitation

Cells on petri dishes or cell pellets were treated with ice-cold 10% trichloroacetic acid (TCA) and transferred into 2 ml polypropylene tubes (Eppendorf; DNA LoBind). Following a 20,000 *g* centrifugation for 3 min at 4°C, supernatant was removed. 1 ml of 5% (*w*/*v*) TCA +10 mM ethylenediaminetetraacetic acid (EDTA) was added to the pellet and vortexed 1 min, after which the sample was centrifuged to 20,000 *g* for 3 min at 4°C and supernatant was removed. We repeated the last step once, and the sample was stored at −80°C. *Neutral Extraction:* Sample tubes containing TCA precipitates were brought to room temperature. Tubes were briefly spun down to remove any residual liquid left. Then 750 µl of chloroform: methanol (1:2, *v*:*v*) were added to the pellet. Samples were vortexed in a small tube mixer (Eppendorf: Thermomixer) at full speed at room temperature and subsequently centrifuged at 20,000 *g* for 5 min at room temperature. The supernatant was discarded. Neutral extraction was repeated once, and the remaining pellets were stored at −80°C to be used for acidic extraction.

Acidic extraction

Internal standards (Avanti polar lipids, 2 ng PIP_3, 20 ng of PIP_2, 20 ng of PIP, 60 ng of PI) were added to the pellets and lipid extraction was initiated with the addition of 726 microliters of chloroform: methanol:12.1 N HCl (40:80:1) after which the samples were vortexed in an Eppendorf Thermomixer at full speed at +4°C for 15 min. Then, 720 µl of chloroform was added and the samples were vortexed for another 5 min after which 354 µl of 1 N hydrochloric acid (HCl) was added and samples vortexed for 2 min. Phases were separated by centrifugation for 5 min at 1,000 *g* at +4°C. The lower phases were collected in a fresh 2 ml tube. An additional 1,098 µl of theoretical lower phase (chloroform: methanol: 1.185 N HCl 86:14:1, *v*:*v*:*v*) was added to the upper phase followed by vortexing and centrifugation at 1,000 *g* for an additional 5 min. The resultant lower phase was combined with the previously collected lower phase and the combination was dried using a refrigerated Labconco Centrivap at −4°C under full vacuum (chamber temperature was brought to room temperature prior to opening the lid at the end). The dried samples were derivatized and phosphoinositides analyzed via liquid chromatography tandem mass spectrometry as described (Traynor-Kaplan *et al*, 2017). Lipid levels were calculated from peak areas normalized to internal standards. *Derivatization method:* Briefly, 100 µL of dichloromethane: methanol:TMS-diazomethane (2.0 M in diethyl ether) 5/4/1 was added to each dry lipid extract to derivatize the extracted lipids through permethylation of the phosphates. The permethylation reaction continued for 1 h at room temperature. The reactions were dried prior to LC-MS/MS analysis in a Centrivap (Labconco) at room temperature under controlled vacuum to prevent solvent bumping. Lipid levels were calculated from peak areas normalized to internal standards.

PIP_3 and $PI(3,4)P_2$ mass ELISA

$PI(3,45)P_3$ (K-2500s) and $PI(3,4)P_2$ (K-3800) mass ELISA kits were purchased from Echelon Biosciences Inc., and the assays were performed according to the manufacturer's protocol. Briefly, 30×10^6 BMDMs were treated with vehicle (DMSO) or 4µ8c (100 µM) for 24 h. Lipid isolation was performed according to the support protocol recommended by the kit protocol. Both $PI(3,45)P_3$ and $PI(3,4)P_2$ were measured from the same sample. OD was measured at 450 nm. $PI(3,4,5)P_3$ and $PI(3,4)P_2$ concentration for the unknown samples was interpolated from the standard curve drawn using sigmoidal 4PL curve analysis with the GraphPad Prism software.

Statistics

Results are reported as mean ± SEM, and statistical significance was determined with Student's *t* test. $P < 0.05$ was considered as * significant.

Data availability

This study includes no data deposited in external repositories.

Expanded View for this article is available online.

Acknowledgements

We are grateful to Dr. Gokhan S. Hotamisligil (Harvard School of Public Health) for providing the mouse embryonic fibroblasts, to Dr. Peter Walter (University of California, San Francisco) for the IRE1 plasmids, and to Dr. Takao Iwawaki (Kanazawa Medical University) for the *IRE1*$^{flox/flox}$ mice. We express our appreciation to all members of Ebru Erbay and Roberta Gottlieb laboratories for insightful discussions on the manuscript. This work was supported by the European Research Council StG 336643 to E.E. European Research Council AdG 692511 and Deutsche Forschungsgemeinschaft (SFB 1123 and TRR 267-A02) to C.W. C.S. and M.C. were partially supported by the Deutsche Forschungsgemeinschaft (DFG Transregio 83 and 186). C.W. is a Van de Laar professor of atherosclerosis. B.K. was partially supported by Fulbright scholarship (FY-2017-TR-PD-01).

Author contributions

EE conceived the study. EE and SMH designed the experiments, with input from the authors. SMH, MC, EMT, IC, ZY, AED, BK, UIO, and AT-K performed experiments. All authors contributed to the data analysis. EE, CS, MA, and CW supervised research. EE and SMH wrote original draft and edited with input from all authors.

Conflict of interest

The authors declare that they have no conflict of interest.

References

Acosta-Alvear D, Karagoz GE, Frohlich F, Li H, Walther TC, Walter P (2018) The unfolded protein response and endoplasmic reticulum protein targeting machineries converge on the stress sensor IRE1. *Elife* 7: e43036

Appenzeller-Herzog C, Hall MN (2012) Bidirectional crosstalk between endoplasmic reticulum stress and mTOR signaling. *Trends Cell Biol* 22: 274 – 282

Backers K, Blero D, Paternotte N, Zhang J, Erneux C (2003) The termination of PI3K signalling by SHIP1 and SHIP2 inositol 5-phosphatases. *Adv Enzyme Regul* 43: 15 – 28

Balla T, Szentpetery Z, Kim YJ (2009) Phosphoinositide signaling: new tools and insights. *Physiology (Bethesda)* 24: 231 – 244

Bartel DP (2004) MicroRNAs: genomics, biogenesis, mechanism, and function. *Cell* 116: 281 – 297

Behrman S, Acosta-Alvear D, Walter P (2011) A CHOP-regulated microRNA controls rhodopsin expression. *J Cell Biol* 192: 919 – 927

Ben-Dror K, Birk R (2019) Oleic acid ameliorates palmitic acid-induced ER stress and inflammation markers in naive and cerulein-treated exocrine pancreas cells. *Biosci Rep* 39: BSR20190054

Ben-Sahra I, Manning BD (2017) mTORC1 signaling and the metabolic control of cell growth. *Curr Opin Cell Biol* 45: 72 – 82

Bernstein E, Caudy AA, Hammond SM, Hannon GJ (2001) Role for a bidentate ribonuclease in the initiation step of RNA interference. *Nature* 409: 363 – 366

Betel D, Wilson M, Gabow A, Marks DS, Sander C (2008) The microRNA.org resource: targets and expression. *Nucleic Acids Res* 36: D149 – D153

Betel D, Koppal A, Agius P, Sander C, Leslie C (2010) Comprehensive modeling of microRNA targets predicts functional non-conserved and non-canonical sites. *Genome Biol* 11: R90

Blackwood EA, Hofmann C, Santo Domingo M, Bilal AS, Sarakki A, Stauffer W, Arrieta A, Thuerauf DJ, Kolkhorst FW, Müller OJ *et al* (2019) ATF6 regulates cardiac hypertrophy by transcriptional induction of the mTORC1 activator, Rheb. *Circ Res* 124: 79 – 93

Brunsing R, Omori SA, Weber F, Bicknell A, Friend L, Rickert R, Niwa M (2008) B- and T-cell development both involve activity of the unfolded protein response pathway. *J Biol Chem* 283: 17954 – 17961

Carreras-Sureda A, Jana F, Urra H, Durand S, Mortenson DE, Sagredo A, Bustos G, Hazari Y, Ramos-Fernandez E, Sassano ML *et al* (2019) Non-canonical function of IRE1alpha determines mitochondria-associated endoplasmic reticulum composition to control calcium transfer and bioenergetics. *Nat Cell Biol* 21: 755 – 767

Chaix A, Zarrinpar A, Panda S (2016) The circadian coordination of cell biology. *J Cell Biol* 215: 15 – 25

Chang HJ, Jones EW, Henry SA (2002) Role of the unfolded protein response pathway in regulation of INO1 and in the sec14 bypass mechanism in *Saccharomyces cerevisiae*. *Genetics* 162: 29 – 43

Cheloufi S, dos Santos CO, Chong MM, Hannon GJ (2010) A dicer-independent miRNA biogenesis pathway that requires Ago catalysis. *Nature* 465: 584 – 589

Chen J, Chen ZJ (2018) PtdIns4P on dispersed trans-Golgi network mediates NLRP3 inflammasome activation. *Nature* 564: 71 – 76

Chendrimada TP, Gregory RI, Kumaraswamy E, Norman J, Cooch N, Nishikura K, Shiekhattar R (2005) TRBP recruits the Dicer complex to Ago2 for microRNA processing and gene silencing. *Nature* 436: 740 – 744

Chung WY, Jha A, Ahuja M, Muallem S (2017) Ca(2+) influx at the ER/PM junctions. *Cell Calcium* 63: 29 – 32

Cimen I, Kocaturk B, Koyuncu S, Tufanli O, Onat UI, Yildirim AD, Apaydin O, Demirsoy S, Aykut ZG, Nguyen UT *et al* (2016) Prevention of atherosclerosis by bioactive palmitoleate through suppression of organelle stress and inflammasome activation. *Sci Transl Med* 8: 358ra126

Cretenet G, le Clech M, Gachon F (2010) Circadian clock-coordinated 12 Hr period rhythmic activation of the IRE1alpha pathway controls lipid metabolism in mouse liver. *Cell Metab* 11: 47 – 57

Diakogiannaki E, Welters HJ, Morgan NG (2008) Differential regulation of the endoplasmic reticulum stress response in pancreatic beta-cells exposed to long-chain saturated and monounsaturated fatty acids. *J Endocrinol* 197: 553 – 563

Duplus E, Glorian M, Forest C (2000) Fatty acid regulation of gene transcription. *J Biol Chem* 275: 30749 – 30752

Elong Edimo W, Ghosh S, Derua R, Janssens V, Waelkens E, Vanderwinden JM, Robe P, Erneux C (2016) SHIP2 controls plasma membrane PI(4,5)P2 thereby participating in the control of cell migration in 1321 N1 glioblastoma cells. *J Cell Sci* 129: 1101 – 1114

Erbay E, Babaev VR, Mayers JR, Makowski L, Charles KN, Snitow ME, Fazio S, Wiest MM, Watkins SM, Linton MF *et al* (2009) Reducing endoplasmic reticulum stress through a macrophage lipid chaperone alleviates atherosclerosis. *Nat Med* 15: 1383 – 1391

Fruman DA, Chiu H, Hopkins BD, Bagrodia S, Cantley LC, Abraham RT (2017) The PI3K pathway in human disease. *Cell* 170: 605 – 635

Getz GS, Reardon CA (2012) Animal models of atherosclerosis. *Arterioscler Thromb Vasc Biol* 32: 1104 – 1115

Gomez JA, Rutkowski DT (2016) Experimental reconstitution of chronic ER stress in the liver reveals feedback suppression of BiP mRNA expression. *Elife* 5: e20390

Halbleib K, Pesek K, Covino R, Hofbauer HF, Wunnicke D, Hanelt I, Hummer G, Ernst R (2017) Activation of the unfolded protein response by lipid bilayer stress. *Mol Cell* 67: 673 – 684

Hara K, Yonezawa K, Weng QP, Kozlowski MT, Belham C, Avruch J (1998) Amino acid sufficiency and mTOR regulate p70 S6 kinase and eIF-4E BP1 through a common effector mechanism. *J Biol Chem* 273: 14484 – 14494

Harnoss JM, le Thomas A, Shemorry A, Marsters SA, Lawrence DA, Lu M, Chen YA, Qing J, Totpal K, Kan D *et al* (2019) Disruption of IRE1alpha through its kinase domain attenuates multiple myeloma. *Proc Natl Acad Sci USA* 116: 16420 – 16429

Hayashi A, Kasahara T, Iwamoto K, Ishiwata M, Kametani M, Kakiuchi C, Furuichi T, Kato T (2007) The role of brain-derived neurotrophic factor (BDNF)-induced XBP1 splicing during brain development. *J Biol Chem* 282: 34525 – 34534

Henry KA, Blank HM, Hoose SA, Polymenis M (2010) The unfolded protein response is not necessary for the G1/S transition, but it is required for chromosome maintenance in Saccharomyces cerevisiae. *PLoS One* 5: e12732

Henry SA, Gaspar ML, Jesch SA (2014) The response to inositol: regulation of glycerolipid metabolism and stress response signaling in yeast. *Chem Phys Lipids* 180: 23 – 43

Hotamisligil GS, Erbay E (2008) Nutrient sensing and inflammation in metabolic diseases. *Nat Rev Immunol* 8: 923 – 934

Hotamisligil GS (2010) Endoplasmic reticulum stress and the inflammatory basis of metabolic disease. *Cell* 140: 900 – 917

Huang J, Manning BD (2009) A complex interplay between Akt, TSC2 and the two mTOR complexes. *Biochem Soc Trans* 37: 217 – 222

Ishiyama J, Taguchi R, Akasaka Y, Shibata S, Ito M, Nagasawa M, Murakami K (2011) Unsaturated FAs prevent palmitate-induced LOX-1 induction via inhibition of ER stress in macrophages. *J Lipid Res* 52: 299 – 307

Iwawaki T, Akai R, Kohno K, Miura M (2004) A transgenic mouse model for monitoring endoplasmic reticulum stress. *Nat Med* 10: 98 – 102

Iwawaki T, Akai R, Yamanaka S, Kohno K (2009) Function of IRE1 alpha in the placenta is essential for placental development and embryonic viability. *Proc Natl Acad Sci USA* 106: 16657 – 16662

Kagawa S, Soeda Y, Ishihara H, Oya T, Sasahara M, Yaguchi S, Oshita R, Wada T, Tsuneki H, Sasaoka T (2008) Impact of transgenic overexpression of SH2-containing inositol 5'-phosphatase 2 on glucose metabolism and insulin signaling in mice. *Endocrinology* 149: 642 – 650

Kanda H, Tateya S, Tamori Y, Kotani K, Hiasa K, Kitazawa R, Kitazawa S, Miyachi H, Maeda S, Egashira K *et al* (2006) MCP-1 contributes to macrophage infiltration into adipose tissue, insulin resistance, and hepatic steatosis in obesity. *J Clin Invest* 116: 1494 – 1505

Kawasaki N, Asada R, Saito A, Kanemoto S, Imaizumi K (2012) Obesity-induced endoplasmic reticulum stress causes chronic inflammation in adipose tissue. *Sci Rep* 2: 799

Kelly TJ, Brummer A, Hooshdaran N, Tariveranmoshabad M, Zamudio JR (2019) Temporal control of the TGF-beta signaling network by mouse ESC MicroRNA targets of different affinities. *Cell Rep* 29: 2702 – 2717

Kim YJ, Guzman-Hernandez ML, Balla T (2011) A highly dynamic ER-derived phosphatidylinositol-synthesizing organelle supplies phosphoinositides to cellular membranes. *Dev Cell* 21: 813 – 824

Kim YK, Kim B, Kim VN (2016) Re-evaluation of the roles of DROSHA, Export in 5, and DICER in microRNA biogenesis. *Proc Natl Acad Sci USA* 113: E1881 – E1889

Knaevelsrud H, Simonsen A (2012) Lipids in autophagy: constituents, signaling molecules and cargo with relevance to disease. *Biochim Biophys Acta* 1821: 1133 – 1145

Korennykh AV, Korostelev AA, Egea PF, Finer-Moore J, Stroud RM, Zhang C, Shokat KM, Walter P (2011) Structural and functional basis for RNA cleavage by Ire1. *BMC Biol* 9: 47

Kunz J, Henriquez R, Schneider U, Deuter-Reinhard M, Movva NR, Hall MN (1993) Target of rapamycin in yeast, TOR2, is an essential phosphatidylinositol kinase homolog required for G1 progression. *Cell* 73: 585 – 596

Lee AH, Iwakoshi NN, Glimcher LH (2003) XBP-1 regulates a subset of endoplasmic reticulum resident chaperone genes in the unfolded protein response. *Mol Cell Biol* 23: 7448 – 7459

Li AC, Binder CJ, Gutierrez A, Brown KK, Plotkin CR, Pattison JW, Valledor AF, Davis RA, Willson TM, Witztum JL *et al* (2004) Differential inhibition of macrophage foam-cell formation and atherosclerosis in mice by PPARalpha, beta/delta, and gamma. *J Clin Invest* 114: 1564 – 1576

Liu D, Liu X, Zhou T, Yao W, Zhao J, Zheng Z, Jiang W, Wang F, Aikhionbare FO, Hill DL *et al* (2016) IRE1-RACK1 axis orchestrates ER stress preconditioning-elicited cytoprotection from ischemia/reperfusion injury in liver. *J Mol Cell Biol* 8: 144 – 156

Manning BD, Cantley LC (2007) AKT/PKB signaling: navigating downstream. *Cell* 129: 1261 – 1274

Manning BD, Toker A (2017) AKT/PKB signaling: navigating the network. *Cell* 169: 381 – 405

Maurel M, Chevet E (2013) Endoplasmic reticulum stress signaling: the microRNA connection. *Am J Physiol Cell Physiol* 304: C1117 – C1126

Mehrpour M, Esclatine A, Beau I, Codogno P (2010) Overview of macroautophagy regulation in mammalian cells. *Cell Res* 20: 748 – 762

Moore KJ, Sheedy FJ, Fisher EA (2013) Macrophages in atherosclerosis: a dynamic balance. *Nat Rev Immunol* 13: 709 – 721

Moore K, Hollien J (2015) Ire1-mediated decay in mammalian cells relies on mRNA sequence, structure, and translational status. *Mol Biol Cell* 26: 2873 – 2884

Ni H, Rui Q, Li D, Gao R, Chen G (2018) The role of IRE1 signaling in the central nervous system diseases. *Curr Neuropharmacol* 16: 1340 – 1347

Oh J, Riek AE, Weng S, Petty M, Kim D, Colonna M, Cella M, Bernal-Mizrachi C (2012) Endoplasmic reticulum stress controls M2 macrophage differentiation and foam cell formation. *J Biol Chem* 287: 11629 – 11641

Onat UI, Yildirim AD, Tufanli O, Cimen I, Kocaturk B, Veli Z, Hamid SM, Shimada K, Chen S, Sin J *et al* (2019) Intercepting the lipid-induced integrated stress response reduces atherosclerosis. *J Am Coll Cardiol* 73: 1149 – 1169

Pagliassotti MJ, Kim PY, Estrada AL, Stewart CM, Gentile CL (2016) Endoplasmic reticulum stress in obesity and obesity-related disorders: an expanded view. *Metabolism* 65: 1238 – 1246

Paraskevopoulou MD, Georgakilas G, Kostoulas N, Vlachos IS, Vergoulis T, Reczko M, Filippidis C, Dalamagas T, Hatzigeorgiou AG (2013) DIANA-microT web server v5.0: service integration into miRNA functional analysis workflows. *Nucleic Acids Res* 41: W169 – W173

Pfaffenbach KT, Nivala AM, Reese L, Ellis F, Wang D, Wei Y, Pagliassotti MJ (2010) Rapamycin inhibits postprandial-mediated X-box-binding protein-1 splicing in rat liver. *J Nutr* 140: 879 – 884

Pineau L, Ferreira T (2010) Lipid-induced ER stress in yeast and beta cells: parallel trails to a common fate. *FEMS Yeast Res* 10: 1035 – 1045

Rameh LE, Mackey AM (2016) IQGAP1 makes PI(3)K signalling as easy as PIP, PIP2, PIP3. *Nat Cell Biol* 18: 1263 – 1265

Reczko M, Maragkakis M, Alexiou P, Grosse I, Hatzigeorgiou AG (2012) Functional microRNA targets in protein coding sequences. *Bioinformatics* 28: 771 – 776

Riera-Borrull M, Cuevas VD, Alonso B, Vega MA, Joven J, Izquierdo E, Corbi AL (2017) Palmitate conditions macrophages for enhanced responses toward inflammatory stimuli via JNK activation. *J Immunol* 199: 3858 – 3869

Ron D, Walter P (2007) Signal integration in the endoplasmic reticulum unfolded protein response. *Nat Rev Mol Cell Biol* 8: 519 – 529

Rutkowski DT, Hegde RS (2010) Regulation of basal cellular physiology by the homeostatic unfolded protein response. *J Cell Biol* 189: 783 – 794

Sanchez-Alvarez M, del Pozo MA, Bakal C (2017) AKT-mTOR signaling modulates the dynamics of IRE1 RNAse activity by regulating ER-mitochondria contacts. *Sci Rep* 7: 16497

Schewe DM, Aguirre-Ghiso JA (2008) ATF6alpha-Rheb-mTOR signaling promotes survival of dormant tumor cells *in vivo*. *Proc Natl Acad Sci USA* 105: 10519 – 10524

Schuck S, Prinz WA, Thorn KS, Voss C, Walter P (2009) Membrane expansion alleviates endoplasmic reticulum stress independently of the unfolded protein response. *J Cell Biol* 187: 525 – 536

Shimobayashi M, Hall MN (2014) Making new contacts: the mTOR network in metabolism and signalling crosstalk. *Nat Rev Mol Cell Biol* 15: 155 – 162

Tabas I, Ron D (2011) Integrating the mechanisms of apoptosis induced by endoplasmic reticulum stress. *Nat Cell Biol* 13: 184 – 190

Thakur PC, Stuckenholz C, Rivera MR, Davison JM, Yao JK, Amsterdam A, Sadler KC, Bahary N (2011) Lack of *de novo* phosphatidylinositol synthesis leads to endoplasmic reticulum stress and hepatic steatosis in cdipt-deficient zebrafish. *Hepatology* 54: 452 – 462

Traynor-Kaplan A, Kruse M, Dickson EJ, Dai G, Vivas O, Yu H, Whittington D, Hille B (2017) Fatty-acyl chain profiles of cellular phosphoinositides. *Biochim Biophys Acta Mol Cell Biol Lipids* 1862: 513 – 522

Tufanli O, Telkoparan Akillilar P, Acosta-Alvear D, Kocaturk B, Onat UI, Hamid SM, Cimen I, Walter P, Weber C, Erbay E (2017) Targeting IRE1 with small molecules counteracts progression of atherosclerosis. *Proc Natl Acad Sci USA* 114: E1395 – E1404

Ueno K, Samura M, Nakamura T, Tanaka Y, Takeuchi Y, Kawamura D, Takahashi M, Hosoyama T, Morikage N, Hamano K (2016) Increased plasma VEGF levels following ischemic preconditioning are associated with downregulation of miRNA-762 and miR-3072-5p. *Sci Rep* 6: 36758

Upton JP, Wang L, Han D, Wang ES, Huskey NE, Lim L, Truitt M, McManus MT, Ruggero D, Goga A *et al* (2012) IRE1alpha cleaves select microRNAs during ER stress to derepress translation of proapoptotic Caspase-2. *Science* 338: 818 – 822

Volmer R, van der Ploeg K, Ron D (2013) Membrane lipid saturation activates endoplasmic reticulum unfolded protein response transducers through their transmembrane domains. *Proc Natl Acad Sci USA* 110: 4628 – 4633

Volmer R, Ron D (2015) Lipid-dependent regulation of the unfolded protein response. *Curr Opin Cell Biol* 33: 67 – 73

Walter P, Ron D (2011) The unfolded protein response: from stress pathway to homeostatic regulation. *Science* 334: 1081 – 1086

Wang DD, Hu FB (2017) Dietary fat and risk of cardiovascular disease: recent controversies and advances. *Annu Rev Nutr* 37: 423 – 446

Wang JM, Qiu Y, Yang Z, Kim H, Qian Q, Sun Q, Zhang C, Yin L, Fang D, Back SH *et al* (2018) IRE1alpha prevents hepatic steatosis by processing and promoting the degradation of select microRNAs. *Sci Signal* 11: eaao4617

Wei Y, Wang D, Topczewski F, Pagliassotti MJ (2006) Saturated fatty acids induce endoplasmic reticulum stress and apoptosis independently of ceramide in liver cells. *Am J Physiol Endocrinol Metab* 291: E275 – E281

Wei Y, Corbalan-Campos J, Gurung R, Natarelli L, Zhu M, Exner N, Erhard F, Greulich F, Geissler C, Uhlenhaut NH *et al* (2018) Dicer in macrophages prevents atherosclerosis by promoting mitochondrial oxidative metabolism. *Circulation* 138: 2007 – 2020

Wu T, Jiang N, Ji Z, Shi G (2019) The IRE1 signaling pathway is involved in the protective effect of low-dose LPS on myocardial ischemia-reperfusion injury. *Life Sci* 231: 116569

Wullschleger S, Loewith R, Hall MN (2006) TOR signaling in growth and metabolism. *Cell* 124: 471 – 484

Yang JS, Lai EC (2011) Alternative miRNA biogenesis pathways and the interpretation of core miRNA pathway mutants. *Mol Cell* 43: 892 – 903

Yu J, Ryan DG, Getsios S, Oliveira-Fernandes M, Fatima A, Lavker RM (2008) MicroRNA-184 antagonizes microRNA-205 to maintain SHIP2 levels in epithelia. *Proc Natl Acad Sci USA* 105: 19300 – 19305

Zhang X, Goncalves R, Mosser DM (2008) The isolation and characterization of murine macrophages. *Curr Protoc Immunol* 83: 14.1.1 – 14.1.14

Zhao Y, Xiang L, Liu Y, Niu M, Yuan J, Chen H (2018) Atherosclerosis induced by a high-cholesterol and high-fat diet in the inbred strain of the wuzhishan miniature pig. *Anim Biotechnol* 29: 110 – 118

Zhou J, Liu CY, Back SH, Clark RL, Peisach D, Xu Z, Kaufman RJ (2006) The crystal structure of human IRE1 luminal domain reveals a conserved dimerization interface required for activation of the unfolded protein response. *Proc Natl Acad Sci USA* 103: 14343 – 14348

Zhou L, Zang G, Zhang G, Wang H, Zhang X, Johnston N, Min W, Luke P, Jevnikar A, Haig A *et al* (2013) MicroRNA and mRNA signatures in ischemia reperfusion injury in heart transplantation. *PLoS One* 8: e79805

Zoncu R, Efeyan A, Sabatini DM (2011) mTOR: from growth signal integration to cancer, diabetes and ageing. *Nat Rev Mol Cell Biol* 12: 21 – 35